Environmental conditions and microbial community structure during the Great Ordovician Biodiversification Event; a multi-disciplinary study from the Canning Basin, Western Australia

Gemma Spaak, Dianne S. Edwards, Clinton B. Foster, Anais Pagès, Roger E. Summons, Neil Sherwood, Kliti Grice

PII: S0921-8181(17)30252-7
DOI: doi:10.1016/j.gloplacha.2017.10.010
Reference: GLOBAL 2664

To appear in: *Global and Planetary Change*

Received date: 16 May 2017
Revised date: 14 October 2017
Accepted date: 26 October 2017

Please cite this article as: Gemma Spaak, Dianne S. Edwards, Clinton B. Foster, Anais Pagès, Roger E. Summons, Neil Sherwood, Kliti Grice , Environmental conditions and microbial community structure during the Great Ordovician Biodiversification Event; a multi-disciplinary study from the Canning Basin, Western Australia. The address for the corresponding author was captured as affiliation for all authors. Please check if appropriate. Global(2017), doi:10.1016/j.gloplacha.2017.10.010

Environmental conditions and microbial community structure during the Great Ordovician Biodiversification Event; a multi-disciplinary study from the Canning Basin, Western Australia

Gemma Spaak[a], Dianne S. Edwards[b], Clinton B. Foster[c,d], Anais Pagès[e,a], Roger E. Summons[f], Neil Sherwood[g], Kliti Grice[a]*

[a]*Western Australian Organic and Isotope Geochemistry Centre (part of The Institute for Geoscience Research), Curtin University, Perth, WA 6845, Australia*

[b]*Geoscience Australia, Canberra, ACT 2609, Australia*

[c]*School of Earth Sciences, The University of Western Australia, Perth, WA 6009, Australia*

[d]*Research School of Earth Sciences, The Australian National University, Canberra, ACT 2601, Australia*

[e]*CSIRO Mineral Resources, Perth, WA 6151, Australia*

[f]*Department of Earth, Atmospheric & Planetary Sciences, MIT, Boston, USA*

[g]*CSIRO Energy, Sydney, NSW 2113, Australia*

*Corresponding author:

Kliti Grice

Curtin University

WA-OIGC – Dept. of Chemistry

GPO Box U1987

Perth, WA 6102 Australia

Phone: +61 (0)8 9266 2474

Email address:

K.Grice@curtin.edu.au

Abstract

The Great Ordovician Biodiversification Event (GOBE) is regarded as one of the most significant evolutionary events in the history of Phanerozoic life. The present study integrates palynological, petrographic, molecular and stable isotopic ($\delta^{13}C$ of biomarkers) analyses of cores from four boreholes that intersected the Goldwyer Formation, Canning Basin, Western Australia, to determine depositional environments and microbial diversity within a Middle Ordovician epicontinental, tropical sea. Data from this study indicate lateral and temporal variations in lipid biomarker assemblages extracted from Goldwyer Formation rock samples. These variations likely reflect changing redox conditions between the upper (Unit 4) and lower (Units 1+2) Goldwyer, which is largely consistent with existing depositional models for the Goldwyer Formation. Cryptospores were identified in Unit 4 in the Theia-1 well and are most likely derived from bryophyte-like plants, making this is the oldest record of land plants in Australian Middle Ordovician strata. Biomarkers in several samples from Unit 4 that also support derivation from terrestrial organic matter include benzonaphthofurans and $\delta^{13}C$-depleted mid-chain *n*-alkanes. Typical Ordovician marine organisms including acritarchs, chitinozoans, conodonts and graptolites were present in the lower and upper Goldwyer Formation, whereas the enigmatic organism *Gloeocapsomorpha prisca* (*G. prisca*) was only detected in Unit 4. The correlation of a strong *G. prisca* biosignature with high 3-methylhopane indices and ^{13}C depleted *G. prisca*–derived chemical fossils (biomarkers) is interpreted to suggest an ecological relationship between methanotrophs and *G. prisca*. This research contributes to a greater understanding of Ordovician marine environments from a molecular perspective since few biomarker studies have been undertaken on age-equivalent sections. Furthermore, the identification of the oldest cryptospores in Australia and their

corresponding terrestrial biomarkers provides further insight into the geographical distribution and evolution of early land plants.

Keywords: Darriwilian, Canning Basin, biomarkers, methanotrophs, *Gloeocapsomorpha prisca*, cryptospores

Graphical Abstract

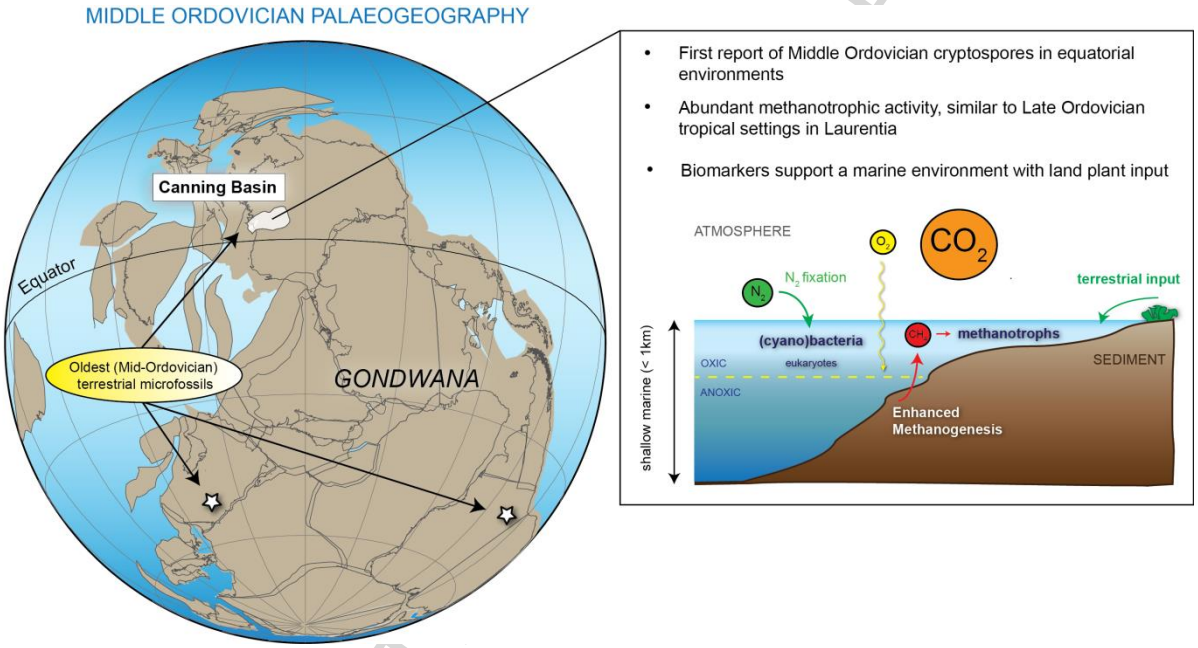

1 Introduction

The Ordovician is a unique time in Earth's history, with characteristically high sea levels and a major increase in marine biodiversity (e.g. Cooper and Sadler, 2004). This rise in biodiversity is commonly referred to as the Great Ordovician Biodiversification Event (GOBE) which, together with the Cambrian Explosion, are the most significant Paleozoic evolutionary events (Cooper and Sadler, 2004; Harper, 2006; Servais et al., 2009). The GOBE has been extensively studied using the fossil record, but far less is known about the biomarker assemblages of Middle Ordovician marine depositional environments. The Darriwilian Goldwyer Formation (Fig. 1, Fig. 2) of the Canning Basin, Western Australia, is one of a few examples of Middle Ordovician sediments on the Australian continent deposited in an equatorial inland sea containing a prolific and diverse microfossil assemblage (Winchester-Seeto et al., 2000; Quintavalle and Playford, 2006a,b; 2008).

During the Ordovician, sea levels were probably higher than at any other time in the Paleozoic (Munnecke et al., 2010) and the expansion of marine habitats was an important stimulus for the diversification. Although the rise in biodiversity predominantly applied to marine organisms, life on land also started to evolve during this time. The Middle Ordovician (Dapingian) records the earliest evidence of land plants in the form of cryptospores—microfossils of presumed bryophyte origin (Rubinstein et al., 2010). Some of these early plants may resemble bryophytes in their size and morphology, but their biology remains largely unknown (Edwards et al., 2014). Recent work by Lenton et al. (2012, 2016) suggests that the appearance of early land plants could have had a significant impact on global climate, potentially contributing to the Late Ordovician cooling and the rise in atmospheric oxygen.

Biomarkers are useful reconstruction tools which provide detailed information on past microbial communities, terrestrial inputs in marine environments, as well as other

palaeoenvironmental conditions such as water column chemistry and stratification (e.g. Peters et al., 2005). Moreover, the study of biomarkers, molecular compounds with specific biosynthetic origins, can reveal further information on the physiology and ecology of extinct taxa (e.g. Hoffmann et al., 1987; Blokker et al., 2001; Gupta et al., 2006; Dutta et al., 2007; Jacob et al., 2007). Of particular interest here is *Gloeocapsomorpha prisca* (*G. prisca*), an organic-walled microfossil of controversial habitat and physiology, which exhibits characteristic geochemical properties and has contributed to many Cambro-Ordovician organic-rich rocks (e.g. Reed et al., 1986; Foster et al., 1986, 1989, 1990; Fowler et al., 2004; Boreham and Ambrose, 2007). Biomarkers also have the potential to identify organisms that are rarely preserved as fossils, such as 3-methylhopanes which are pertinent to detect the presence of methanotrophs (e.g. Farrimond et al., 2004 and references therein). Coupling biomarker studies with compound-specific isotope analyses can provide further insight into organic matter sources, microbial communities and biogeochemical cycles.

The primary aim of the present study is to provide further understanding of Middle Ordovician microbial community structure from a molecular perspective. The Goldwyer Formation is an analogue for Middle Ordovician epeiric tropical environments, and the multi-disciplinary approach allows for integration of molecular signatures with micro- and macrofossils. This paper presents data from molecular and compound-specific stable isotopic ($\delta^{13}C$ of biomarkers) analyses together with palynological and petrological studies to understand the relationships between palaeoenvironment, microbial communities, and the type of organic matter preserved within the marine sediments.

2 Geological background

The Canning Basin, located in the northwestern part of Western Australia (WA) (Fig. 1), is the largest onshore sedimentary basin in that state covering an area of about 430,000 km^2 (Triche and Bahar, 2013). The basin contains rocks of Ordovician to Cretaceous age (Forman and Wales, 1981; Kennard et al., 1994). Deposition began in the Early Ordovician as a consequence of extensional tectonics, with rapid subsidence during the Early–Middle Ordovician resulting in the onset of marine conditions (Romine et al., 1994). Macro- and microfossils from the Middle Ordovician Goldwyer Formation corroborate a shallow marine depositional environment (Winchester-Seeto et al., 2000; Haines, 2004; Quintavalle and Playford, 2006a,b; 2008). By the Late Ordovician, subsidence ceased and marginal marine and evaporitic conditions were established. Smaller scale transgressive-regressive cycles are superimposed on this broad regional trend (Haines, 2004).

Four informal lithologic units (designated Units 1 to 4) have been described for the Goldwyer Formation by Foster et al. (1986) in the eastern Canning Basin. Palynological assemblage zones roughly correlate to these lithological units (Quintavalle and Playford, 2006b), as shown in Figure 2. In a sequence stratigraphic framework, the lower Goldwyer succession (Units 1+2) records a major transgression affecting most of the basin that deposited open marine mudstones over 700 m thick in basinal areas and condensed-section carbonates on platforms and terraces. The onset of the transgression is shown by an abrupt increase in petrophysical borehole electric-log measurement of gamma radiation in Goldwyer-1 and Theia-1 (Fig. 1). The transgression was followed by a slow regressive phase with the deposition of outer shelf to fore slope facies (Romine et al., 1994; Haines, 2004). A smaller scale regression resulted in the deposition of a carbonate-dominated succession (Unit

3), followed by another transgression with the deposition of the upper Goldwyer Formation (Unit 4), that can also be observed in the gamma-ray logs (Fig. 1).

For the present study, the lower and upper calcareous mudstone units of the Goldwyer Formation were sampled in four wells from west to east: Goldwyer-1, Theia-1, Santalum-1A and Solanum-1. Santalum-1A and Solanum-1 intersect a more limestone-dominated succession in comparison to the mudstone-dominated sediments intersected in Goldwyer-1, and Theia-1, especially in relation to Unit 4, indicating shallower conditions on the more southeastward part of the Broome Platform (Haines, 2004). The carbonates from Unit 4 in Solanum-1 and Santalum-1A are bioturbated whereas the samples from Units 1+2 and Unit 4 in Goldwyer-1 and Theia-1 comprise grey-black mudstone with no obvious bioturbation. Further sample description is provided in the supplementary online material (SOM).

3 Materials and Methods

3.1 Sampling strategy and preparation

To investigate the depositional environment of the Goldwyer Formation, cores from Goldwyer-1, Santalum-1A, Solanum-1 and the recently drilled well, Theia-1 (Finder Exploration Pty Ltd, 2015) were sampled (Table 1). As noted above, four informal rock units have been recognised in the Goldwyer Formation (Units 1 to 4; Foster et al., 1986); however, the shale-rich sections of Unit 1 and Unit 2 of the lower Goldwyer Formation could not be separated in Theia-1 and hence are agglomerated. Unit 3, composed predominantly of carbonate, was not sampled due to its low TOC contents. Unit 4 of the upper Goldwyer Formation was sampled most frequently based on previous records of the distinctive palynomorph *G. prisca*. Sample selection from Units 1+2 and Unit 4 was based on:

availability of core; previously measured total organic carbon (TOC) contents (> 1 wt. %); and, for three wells, evidence of low thermal maturity from existing Rock-Eval data and maceral reflectance values. Organic matter from Theia-1 is the most thermally mature, and samples with high TOC were selected. Sample material was obtained from core stored at the Geological Survey of Western Australia core library.

Ensuring hydrocarbon syngeneity in ancient rocks is crucial to avoid misinterpretation of the biomarker signatures (e.g. Brocks et al., 2003). Once the cut core samples were obtained from the core library, special precaution was taken to minimise further surface contamination. Rock samples were surface washed several times with organic solvents to remove surface contamination prior to grinding. Procedural blanks were adopted throughout the washing, grinding and extraction process to avoid (cross) contamination. The protocol for sample preparation and extraction is described in detail in the SOM.

3.2 Analytical methods

Rock-Eval pyrolysis, organic petrology, palynology and organic geochemical analyses were undertaken following published, standardised methods which are described in the SOM.

4 Results and Interpretation

4.1 Palynology

Palynological analyses, using standard processes, were carried out on selected samples from Units 1+2 and Unit 4 in all four wells. Palynomorph assemblages and some selected key species are summarised in Table 2 and illustrated in Figure 3. The results indicate a marine

depositional environment with rare evidence of land-plant input in Unit 4. The marine microfossils include: scolecodonts (worm jaw fragments,Fig. 3a), chitinozoans (Fig. 3b), graptolite fragments (Goldwyer-1, Fig.3c), spinose acritarchs (Fig. 3d-f), and *G. prisca* colonies (Theia-1, Santalum-1A and Solanum-1, Fig. 3g). Quintavalle and Playford (2006, 2008) provide the most recent and comprehensive systematic accounts of Ordovician palynofloras from the Canning Basin. Winchester-Seeto et al. (2000, 2001) also described chitinozoa from the Goldwyer and Nita formations and related quantitative abundances of these microfossils with small scale transgressive-regressive cycles in Unit 4 of Santalum-1A.

Key differences are noted between our samples from Units 1+2 and Unit 4 (Table 2). *G. prisca* microfossils are only observed in Unit 4 and the samples from Units 1+2 comprise dark to very dark brown organic debris with chitinozoan and graptolite fragments and rare acritarchs and leiosphaerids. As reviewed by Quintavalle and Playford (2006b, 115-124), the age of the Goldwyer Formation, as determined from associated faunal elements (trilobites, graptolites, and conodonts) is Middle Ordovician, Darriwilian (= Llanvirn). *Inter alia*, the co-occurrence of *Dasydorus cirritus*, *Sacculidium aduncum* (Fig. 3d), *Pirea* sp. cf. *P. ornata* (Fig. 3e), *Striatotheca indistincta* (Fig. 3f), and in the assemblage from Theia-1 core (1217.7-1217.67 m) confirms correlation with palynofloras from the Goldwyer Formation (see Quintavalle and Playford 2006b).

Cryptospores were found in Unit 4 of Theia-1 (1217.67–1217.7 m), occurring as both dyads and tetrads, and all in enclosed envelopes (Fig. 3i). The tetrads exhibit strong similarities to an undescribed Dapingian cryptospore previously identified in samples from Argentina (Rubinstein et al., 2010). A single specimen appears to exhibit a trilete mark (Fig. 3h), with thickened laesurae (sutures), and thereby differs from those reported by Steemans et al. (2009). However, if this is a true trilete spore, it would predate the current oldest occurrence of trilete spores (late Katian/Hirnantian) by ca. 20 Ma (Steemans et al., 2009).

4.2 Organic Petrology

Organic petrological analyses undertaken in both white light and ultraviolet/blue light (fluorescence mode) showed that the macerals in Unit 4 at Solanum-1 and Santalum-1A comprise common fluorescing liptinite and rare vitrinite-like faunal remains, probably at least in part derived from graptolites (Sherwood and Li, 2016), as shown in Figure 4. The liptinite in most samples from Solanum-1 comprises acritarch-derived lamalginite, along with lesser amounts of liptodetrinite and telalginite derived from *G. prisca* (Fig. 4b-c). Liptinite in the lowermost sample (~490 m depth) from Santalum-1A occurs mainly as telalginite, derived from *G. prisca* (Fig. 4a), along with sparse acritarch-derived lamalginite.

The uppermost sample (973 m) from Unit 4 in Goldwyer-1 contains rare fluorescing liptodetrinite and lamalginite derived from acritarchs. In contrast, the organic matter in the samples from Units 1+2 in this well comprises non-fluorescing, finely disseminated bitumen with rare to sparse vitrinite-like faunal remains exhibiting characteristics similar to that of chitinozoans and graptolites (Fig. 4d).

4.3 Organic richness and thermal maturity

Rock-Eval pyrolysis results are summarised in Table 1. The Goldwyer Formation samples from Unit 4 contain type II kerogen with TOC contents up to 3.6 wt. %. Bitumen and faunal reflectance range between 0.5 and 0.7% (Table 1). Bitumen and faunal reflectance is used widely to determine maturity in early Paleozoic sediments where vitrinite is either scarce or absent, and this technique has been applied to the Goldwyer Formation samples (Sherwood and Li, 2016). On the basis of conversions of bitumen reflectance to vitrinite reflectance from

Schoenherr et al. (2007) and considerations of differences between faunal reflectance and vitrinite reflectance from Hartkopf-Fröder et al. (2015), the maceral reflectance indicate that Unit 4 is in the early stage of oil generation. The organic matter preserved in Units 1+2 at Goldwyer-1 and Theia-1 are also classified as type II kerogen, with a maximum TOC content of 4.5 wt. % (Fig 1). Slightly higher thermal maturities are observed in these samples (maceral reflectance of 0.8–1.5%). In Theia-1, maceral reflectance values are >1% and the absence of hopanes and steranes corroborate high thermal maturity (in the main stage of gas generation). However, Tmax values are suppressed in this well due to the presence of generated hydrocarbons, as determined by the high production index (0.2 > PI < 0.38) (Table 1: Finder Exploration Pty Ltd, 2015).

4.4 Aliphatic and aromatic hydrocarbons

All aliphatic hydrocarbon fractions contain abundant short to mid chain length *n*-alkanes (C_{12} [occasionally], C_{14} to C_{23}), with some samples showing additional contributions of longer chain *n*-alkanes (up to C_{33}) (Fig. 5). The isoprenoids pristane (Pr) and phytane (Ph) were consistently present but varied in abundance throughout the samples (Fig. 5, Table 3). The C_{27}–C_{35} hopanes and C_{26}–C_{30} steranes were below detection limit in full scan GC-MS analysis and were identified using selected ion monitoring (SIM) mode and multiple reaction monitoring (MRM) GC-MS (Fig. 6, S1, S2, S3 and S4). The aromatic hydrocarbon fractions were dominated by naphthalene, phenanthrene and their methylated derivatives. A detailed account of the *n*-alkane, hopane and sterane assemblages and aromatic compounds is provided in the SOM. Compound specific carbon isotope ($\delta^{13}C$) analysis was performed upon *n*-alkanes from selected samples (Table 4). Samples from Units 1+2 displayed slightly lower *n*-alkane $\delta^{13}C$ values (–31.3 to –33.8‰) than samples from Unit 4 (–27.1 to –32.3‰). In Unit

4 of Santalum-1A, the C_{14}–C_{20} *n*-alkanes were more enriched (–27.1 to –29.4‰) than the C_{25}–C_{32} *n*-alkanes (–29.9 to –32.3‰). Trends in the $\delta^{13}C$ values are illustrated in Figure 7, 8, 9 and S5. The most important molecular and isotopic signatures are summarised in Table 5, together with their biological and environmental interpretation.

5 Discussion

5.1 Evidence of water-column stratification and anoxia

Molecular proxies indicative of environmental conditions are displayed in Fig. 10 and listed in Table 3 and Table 5. The Pr/Ph ratio, dibenzothiophene/phenanthrene (DBT/P) ratio and C_{35} homohopane index are commonly used redox indicators (Didyk et al., 1978; Hughes et al., 1995; Peters et al., 2005). An elevated gammacerane index is indicative of a stratified water column (Moldowan et al., 1985; Sinninghe Damsté et al., 1995; Tulipani et al., 2015). The samples from Unit 4 in Santalum-1A and Solanum-1 on the eastern part of the Broome Platform, contained low gammacerane indices (<0.1) and low C_{35} homohopane indices (average of 0.04) (Fig. 10), suggesting deposition under relatively oxygenated conditions with enhanced water column circulation, which is corroborated by the presence of bioturbation in these sediments.

Although there are fewer data from Units 1+2 in comparison to Unit 4, these samples displayed higher gammacerane indices (0.3–0.7) (Fig. 10) and slightly higher C_{35} homohopane indices (average of 0.06). However, the Pr/Ph ratio and DBT/P ratio do not exhibit distinct differences between Unit 4 and Units 1+2 (Fig. 10). Nonetheless, due to sedimentological features such as laminations and only occasional bioturbation, deposition of Units 1+2 likely occurred under less oxygenated conditions. Deposition of Units 1+2 occurred during a maximum transgression (Romine et al., 1994) and sedimentological features such as high TOC content, laminations and only occasional bioturbation suggests anoxic bottom waters. In this case, decreased oxygenation is likely a result of deeper water conditions facilitated by the transgression. However, this hypothesis does not account for topographic variations along the Broome Platform. Silty lenses in the upper part of Units 1+2

at Theia-1 suggest wave action on a muddy shelf. Due to the size of the basin, distance between sampled wells and the low sampling density of Units 1+2, it remains difficult to infer relationships between molecular redox proxies and the geological framework.

The presence of hydrogen sulfide within the sunlight zone of the water column and/or at the sediment/water interface is known as photic zone euxinia (PZE). Phototrophic sulfur bacteria such as Chlorobiaceae flourish in such conditions (Grice et al., 2005; Schwark and Frimmel, 2004). Commonly used biomarkers of Chlorobiaceae include chlorobactane, isorenieratane, palaerenieratane and their derivatives, the aryl isoprenoids with corresponding enriched $\delta^{13}C$ values (Summons and Powell, 1987; Grice et al., 1996). Biomarkers for PZE have been identified in some (restricted) Ordovician–Silurian settings (Koopmans et al., 1996; Pancost et al., 1998; Vandenbroucke et al., 2009; Smolarek et al., 2017). In this study, trace amounts of palaerenieratane and isorenieratane were identified in Solanum-1 at 316.2–316.3 m and in Theia-1 at 1552.7–1552.75 m and aryl isoprenoids of uncertain origin in others (SOM). The low abundance of aryl isoprenoids and aromatic C_{40} carotenoids possibly suggest short periods of PZE, but mixing and oxygenation of the water column must have been frequent to prevent the development of PZE for prolonged periods of time.

5.2 Microbial communities inferred from hopane and sterane distributions

The ratio of the C_{27} to C_{35} hopanes to C_{27} to C_{29} steranes (H/St) generally reflects the balance of bacterial *versus* eukaryotic contributions to sedimentary organic matter. Hopanes are the molecular fossils of hopanoids produced by diverse groups of bacteria, whilst steranes are derived from sterols common to all eukaryotes and are generally absent in bacteria, with few exceptions (Volkman, 1986, 2006; Summons et al., 2006). Further information on bacterial and algal populations can be obtained from the distributions and relative abundances of the

C_{31} 2α- and 3β-methylhopanes and the C_{27}, C_{28} and C_{29} steranes. Figure 10 shows variations in the H/St ratios *versus* methylhopane abundance between Units 1+2 and Unit 4.

In Unit 4, high H/St ratios (H/St average of 6.7) are observed, reflecting a strong predominance of bacteria. These values are significantly above the global average (0.5–2.0) of Phanerozoic marine oils and sediments (Peters et al., 2005). During the Ordovician, fixed nitrogen content of the oceans was low due to extensive denitrification (LaPorte et al., 2009; Melchin et al., 2013; Rohrssen et al., 2013). Eukaryotic algae commonly require a steady supply of fixed nitrogen, and such environmental conditions would have limited their presence in Ordovician oceans (LaPorte et al., 2009). Unit 4 also exhibited high 3-methylhopane abundances, illustrated by high 3-methylhopane indices and low 2-methylhopane/3-methylhopane ratios (Fig. 10, Table 3). Both methanotrophic bacteria and acetic acid bacteria have the ability to produce 3-methylhopanoids (Farrimond et al., 2004; Welander and Summons, 2012), but the presence of acetic acid bacteria would be unlikely in such carbonate-rich, marine environments. The high 3-methylhopane abundance in Unit 4 is interpreted to be indicative of aerobic methanotrophic bacteria, which is consistent with the relatively oxygenated character of the water column under which the sediments within Santalum-1A and Solanum-1 were deposited. Methanotrophic bacterial activity implies the presence of methane in aerobic waters. An enhanced methane cycle has been proposed by Rohrssen et al. (2013) and is thought to have facilitated the presence of methanotrophs. In marine sediments characterised by low concentrations of oxygen and other electron acceptors such as nitrate and sulfate, methanogenesis can account for a significant proportion of organic matter diagenesis. Under such conditions anaerobic oxidation of methane via either sulfate or nitrate reduction would have been low, allowing a greater proportion of methane to escape from the sediments into the water column. In comparison to the present-day, Ordovician oceans were characterised by low concentrations of oxygen, nitrate and sulfate (Gill et al.,

2007; LaPorte et al., 2009; Hammarlund et al., 2012; Thompson and Kah, 2012) and diagenetic methane cycling likely played an important role during deposition of the upper Goldwyer Formation, signified by the abundance of methanotrophic bacteria, especially in Unit 4. A graphical representation of the microbial community present during deposition of Unit 4 is provided in Figure 11.

The samples from Units 1+2 display significantly lower H/St ratios (<2) compared to Unit 4, accompanied with relatively elevated 2-methylhopane abundances. Enhanced levels of fixed nitrogen could have resulted from greater cyanobacterial contributions shown by the relatively elevated 2-methylhopane abundance (Summons and Jahnke, 1990; Summons et al., 1999; Farrimond et al., 2004). This could have enhanced algal productivity, reflected in the lower H/St ratios. Although the presence of 2-methylhopanes in sediments is often correlated to cyanobacteria, several other modern-day bacteria are known to produce 2-methylhopanoids (Ricci et al., 2014) which inhabit a multitude of modern environments. These environments are characterised by suboxia or anoxia, high osmolarity and limited fixed nitrogen (Ricci et al., 2014), which is in agreement with the reducing character of Units 1+2. In this case, the high relative 2-methylhopane abundance can reflect both an increase in cyanobacterial abundance and low oxygen levels.

Steranes are biomarkers for algae and most likely acritarchs (e.g. Talyzina et al., 2000; Volkman, 2006). Acritarch microfossils have been identified in Unit 4 (Table 2, Fig. 3) in this study and in previous studies of the Goldwyer Formation (Winchester-Seeto et al., 2000; Quintavalle and Playford, 2006b). The absence of acritarch microfossils in some samples from Units 1+2 in this study may be due to sampling bias because relatively few samples were subjected to palynological analysis. Thus, the sterane assemblages are inferred to be indicative of algal as well as acritarch contributions to the biomass in Units 1+2 and Unit 4. Common steranes (C_{27}, C_{28} and C_{29}), dinosteranes and 4α-methyl-24-ethylcholestanes have

been identified in numerous acritarch microfossils (e.g. Arouri et al., 2000; Talyzina et al., 2000). Dinosterane (4α,23,24-trimethylcholestane) and 4α-methyl-24-ethylcholestanes were detected in selected samples from Units 1+2 and Unit 4 at varying abundances (Fig. 6, Table 3), which could be related to different acritarch communities. A suite of 24-*n*-propylcholestanes, biomarkers for pelagophyte microalgae (Table 5), were present in Unit 4 but not detected in Units 1+2 (Fig. 6). Pelagophyte microalgae first appeared during the Neoproterozoic to Paleozoic, but there are two hiatuses of the C_{30} sterane biomarkers in the marine rock record from Middle–Late Cambrian and Late Ordovician–early Silurian (Rohrssen et al., 2015). In the Goldwyer Formation, C_{30} sterane abundances reach 3.1% (Table 3), which is higher than the maximum values observed during the Late Ordovician (up to 1.2%, Rohrssen et al., 2015).

The C_{27}:C_{28}:C_{29} sterane distribution in Lower Paleozoic marine deposits is generally characterised by either equal amounts of C_{27} and C_{29} steranes or a predominance of C_{29} steranes (Grantham and Wakefield, 1988; Schwark and Empt, 2006;), although, a strong predominance of C_{27} steranes has been noted in certain Upper Ordovician marine sections (Mustafa et al., 2015; Smolarek et al., 2017). In the upper Goldwyer, the percentages of C_{27} steranes (of $C_{27\text{-}29}$ steranes) vary from ca. 30% to 50%, the percentages of C_{28} steranes vary from ca. 14% to 27%, and the percentages of C_{29} steranes vary from ca. 22% to 52% (Table 3). In Solanum-1, variations are evident in the C_{27}:C_{28}:C_{29} sterane distribution throughout Unit 4 (Fig. 12) possibly relating to changes in algal/acritarch populations, with a predominance of the C_{27} steranes being coincident when sterane abundance is lowest (H/St >6), and there is increased preservation of *G. prisca.* In the lower Goldwyer Formation the percentage of C_{29} steranes is slightly higher (ca. 46% to 54%) than that in the upper Goldwyer Formation (ca. 22% to 52%), providing further indication that different biological communities were present during deposition of Units 1+2 and Unit 4.

5.3 Gloeocapsomorpha prisca

Microfossils characteristic of *G. prisca* were identified in Unit 4 of Theia-1, Solanum-1 and Santalum-1A (Fig. 3, Fig. 4, Table 2). Hydrocarbon fractions of *G. prisca*-rich rocks typically contain distinctive odd-carbon-numbered *n*-alkanes in the C_{15} to C_{19} range with minor contributions of C_{20+} *n*-alkanes, abundant odd-carbon-numbered *n*-alkylcyclohexanes, low contributions of acyclic isoprenoid hydrocarbons, a strong predominance of hopanes *versus* steranes and abundant long-chain alkylnaphthalenes and alkylbenzenes (e.g. Hoffmann et al., 1987; Guthrie and Pratt, 1995; Fowler et al., 2004). The typical odd-over-even *n*-alkane signature of *G. prisca* was observed in selected Unit 4 samples from Goldwyer-1, Theia-1, Santalum-1A and Solanum-1, with varying prevalence. For example, the *n*-alkane odd-over-even predominance (OEP) was present at the base of Unit 4 for Solanum-1 (Fig. 5a), less abundant in the Theia-1 samples (likely due to higher maturity) (Fig. 5e) and absent in the Santalum-1A samples (Fig. 5b). Comparison of *n*-alkane profiles from Solanum-1 samples where *G. prisca* has been quantified (Sherwood and Li, 2016) showed that the *n*-alkane OEP only became prominent when the *G. prisca* liptinite visual abundance was at least 5% of the sample. The $\delta^{13}C$ values of *n*-alkanes in the Solanum-1 samples showed a shift towards more depleted carbon isotopic signatures when *G. prisca* is abundant (Fig. 12), and the odd-carbon numbered *n*-C_{17} and *n*-C_{19} were more depleted in ^{13}C (–31.4‰) in comparison to the *n*-C_{16} and *n*-C_{18} alkanes (–30.0‰) (Fig. 7). These results suggest that the depleted isotopic signature is related to the aliphatic biopolymer of *G. prisca*, which is the predominant source of the *n*-C_{17} and *n*-C_{19} alkanes.

In Unit 4 of Solanum-1, high abundances of *G. prisca*, shown as a pronounced OEP, correlated with TOC abundance equal or greater than 1 wt. %, Pr/Ph ratios >1, lower C_{35}

homohopane indices, elevated H/St ratios, increased 3-methylhopane indices and depleted carbon isotopic signatures of the individual *n*-alkanes (Fig. 12). Furthermore, these intervals were characterised by a change in sedimentation from carbonate to mud-dominated and bioturbation became less prominent, as observed in the "hylogged" core section (Fig. S6). Elevated TOC contents indicate anoxic bottom waters. The disparity between elevated TOC contents and relatively high Pr/Ph ratios and low homohopane indices has been noted previously in the *G. prisca*-rich Guttenberg Member from Iowa (Pancost et al., 1998). In the Guttenberg Member, *G. prisca* makes up 45 to 95 % of the organic matter and it is argued that dense layers of *G. prisca* limited the production of sedimentary hydrogen sulfide. This would have enhanced the preservation of phytol and bacteriohopanetetrol, rationalising relatively high Pr/Ph ratios and low homohopane indices in comparison to sections above and below the Guttenberg Member (Pancost et al., 1998). In the present study, *G. prisca* abundances are much lower and such an explanation cannot be employed. Marine carbonates are commonly associated with high homohopane indices (Peters et al., 2005) and a change from carbonate- to mud-dominated sedimentation is likely driving the observed shift in homohopane index. Likewise, variations in source inputs to Pr and Ph could account for the slight increase in Pr/Ph ratio. Anoxic to dysoxic bottom waters would have promoted methanogenesis and subsequently increased the methane flux into the water column, allowing for an increase in methanotrophs, reflected in increased 3-methylhopane indices (Fig. 12). Rapid sedimentation and burial of refractory *G. prisca* microfossils likely resulted in preservation of organic matter in a predominantly oxygenated water column.

Lipids derived from aerobic methanotrophs are known to be significantly depleted in $\delta^{13}C$ (Summons et al., 1994). In Unit 4 of Solanum-1, the co-occurrence of (i) *G. prisca* biosignatures, (ii) increased 3-methylhopane indices and (iii) depleted carbon isotopic signatures (Fig. 12) suggests a relationship between *G. prisca* and methanotrophs. In the

Guttenberg Member, *G. prisca* biomass is significantly enriched in ^{13}C relative to that of other photoautotrophic organisms (Pancost et al., 1999) and *G. prisca*-derived bitumens from North America exhibit enriched $\delta^{13}C$ values for *n*-C_{17} and *n*-C_{19} relative to the even numbered *n*-alkanes, which is the opposite to these values in the Solanum-1 samples (Fig. 8). In the Guttenberg Member equal amounts of 3- and 2-methylhopanes were recorded (Pancost et al., 1998), whereas the Solanum-1 rock extracts show a distinct predominance of 3-methylhopanes (3MHI of 9-15%) relative to the 2-methylhopanes (2MHI of 3-7%) (Fig. 12). Hence, it seems likely that *G. prisca* utilised carbon ultimately derived from either methane or aerobic methanotrophs resulting in ^{13}C-depleted *n*-alkanes. Similar *n*-alkane carbon isotopic profiles (as shown in Fig. 8) are noted in oils sourced by *G. prisca* in the Canning and Amadeus basins (Edwards et al., 2013; Jarrett et al., 2016) and a predominance of 3-*versus* 2-methylhopane is recorded in oil (Dodonea-1) sourced by this unit (Edwards et al., 1995). These results suggest that the association between methanotrophs and *G. prisca* may not have been a local phenomenon. Although the uptake of ^{13}C depleted carbon via methanotrophs is thought to be the most plausible explanation for the observed isotopic shifts in Solanum-1, other processes (e.g. recycling of CO_2) may have played a role. Nonetheless, the carbon isotopic variations in Australia and North America (Fig. 8) are significant and further investigation is needed to elucidate the underlying biogeochemical processes associated with *G. prisca*.

Nitrogen isotopes of *G. prisca*- rich sedimentary rocks, including samples from the Goldwyer Formation, have been reported previously (Kiipli and Kiipli, 2013) which exhibited average $\delta^{15}N$ values of +7.4‰. Relative to the atmospheric N_2 source (0‰), denitrification in the water column leads to a much larger isotopic fractionation (~20‰) than microbial nitrogen fixation (<3‰) (Luo et al., 2016). These results indicate that denitrification occurred when *G. prisca* was abundant, suggesting *G. prisca* was a nitrate

using not N_2-fixing microorganism (Kiipli and Kiipli, 2013). Cyanobacteria and aerobic methanotrophs have the ability to fix atmospheric nitrogen, thus providing a potential nitrogen source for *G. prisca*.

5.4 Significance of microfossils and terrestrial biomarkers

Land-plant input is evident from the presence of cryptospores and, potentially, a trilete spore in Unit 4 of Theia-1 (Fig. 3). Palynological studies have been performed on the Goldwyer Formation (e.g. Foster et al., 1986; Winchester-Seeto et al., 2000; Quintavalle and Playford, 2006a,b; 2008 and references therein) but this is the first study to find probable land-plant spores. Because of the scarcity of records of land-plant spores within the upper Goldwyer Formation, we suggest that the terrestrial palynomorphs found in Theia-1 are locally derived rather than long distance transport from the hinterland. Palaeogeographic maps indicate the presence of peritidal environments on the Broome Platform (Romine et al., 1994) and periodic exposure of these areas would have allowed for the formation and development of terrestrial life.

To date, the earliest uncontroversial record of land plants (embryophytes) is Early-Middle Ordovician (Dapingian) (Rubinstein et al., 2010), predating the Goldwyer Formation. The samples of the present study therefore provide an exceptional opportunity to investigate terrestrial inputs of organic matter during the Ordovician and potentially identify biomarker signals of early land-plants. Middle to Late Ordovician terrestrial organisms and ecosystems most likely comprised microbial mats, bryophytes/bryophyte-like plants and fungi (Redecker et al., 2000; Wellman and Gray, 2000). The fungi and spores identified in this period indicate that soil development was sufficient to support early bryophytes (Redecker et al., 2000). Little is known about terrestrially sourced aliphatic and aromatic biomarker signatures of Ordovician plants (e.g. see Romero-Sarmiento et al., 2011). Most commonly used terrigenous proxies for Upper Paleozoic to recent sediments include long-chain *n*-alkanes derived from plant waxes (Eglinton and Hamilton, 1967), degradation products from conifer resins (e.g. Otto and Simoneit, 2001), and the carbon isotopic composition of plant-derived mid- to long-

chain *n*-alkanes (Rieley et al., 1991; Bird et al., 1995; Naraoka and Ishiwatari, 1999; Chikaraishi and Naraoka, 2003; Eley et al., 2016).

Modern bryophytes (e.g. *Sphagnum* mosses) and aquatic macrophytes are common sources for odd-carbon-numbered mid-chain *n*-alkanes (C_{21}, C_{23}, C_{25}), and their relative abundance can be used to trace macrophytes and/or bryophytes in ancient deposits (e.g. Ficken et al., 2000; Mead et al., 2005; McKirdy et al., 2010; Tulipani et al., 2014; Inglis et al., 2015). Some samples from Santalum-1A had alkane distributions that are dominated by mid-chain *n*-alkanes (Fig. 5b, 5e-f, 9, S5). One of these samples also exhibited a slight OEP at *n*-C_{25} and *n*-C_{27} (Fig. 5b), a typical bryophyte signature (e.g. Inglis et al., 2015). Stable carbon isotopes of *n*-$C_{23–32}$ are more depleted in $\delta^{13}C$ (average of –31.0‰) than *n*-$C_{16–19}$ (average of –27.8‰), suggesting that different sources are contributing to the short-chain and mid-chain *n*-alkanes (Fig. 9, Fig. S5). To further assess the significance of this isotopic discrepancy, the difference in $\delta^{13}C$ between short- and mid-chain *n*-alkanes was calculated (Table 6). These values show that the isotopic shift towards depleted $\delta^{13}C$ values is greater in the Santalum-1A samples ($\delta^{13}C$(*n*-$C_{16–19}$) – $\delta^{13}C$(*n*-$C_{23–32}$) = 2.3 to 4‰) in comparison to the samples from Solanum-1, Goldwyer-1 and Theia-1 ($\delta^{13}C$(*n*-$C_{16–19}$) – $\delta^{13}C$(*n*-$C_{23–32}$) = –0.3 to 1.5‰). Taking into account the geological context and presence of land-plant spores, non-vascular C3 plants (i.e. bryophytes or aquatic macrophytes) are thought to have contributed to the mid-chain *n*-alkanes preserved in the upper Goldwyer Formation at Santalum-1A. Possible explanations for the depleted mid-chain *n*-alkane signature include: (i) atmospheric CO_2 may have been depleted which is readily reflected in bryophyte $\delta^{13}C$ as these plants lack stomata to regulate their resistance to inwards CO_2 diffusion (e.g. Royles et al., 2014), or (ii) bryophyte biosynthesis of lipids underlies fractionation of the *n*-alkanes (e.g. Brader et al., 2010). A third possibility may be that bryophytes use recycled and isotopically depleted CO_2

from methanotrophs, which is well known from modern-day environments (Kip et al., 2010; Nichols et al., 2014).

High abundances of benzonaphthofurans were present in the Theia-1 sample from 1217.67–1217.7 m, which also contained the terrestrial palynomorphs. Although the origin of oxygenated heterocyclic aromatic compounds such as dibenzofurans and benzonaphthofurans is still unknown, these compounds prevail in terrestrial sediments and previous studies have suggested a land plant origin (Sephton et al., 2005; Versteegh and Riboulleau, 2010; Li and Ellis, 2015;). In this case, the co-occurrence of benzonaphthofurans with the cryptospores and the absence of these aromatic compounds in other Goldwyer Formation samples points towards a common terrestrial source.

5.5 Regional and global correlations of the Goldwyer Formation

This study investigated palaeoenvironmental conditions associated with the deposition of the Middle Ordovician Goldwyer Formation in the Canning Basin, Western Australia. As no biomarker studies are known from age-equivalent sections elsewhere in the world, little can be said about the (geographical) diversity of biomarkers during the Darriwilian. However, the results of this study can be compared to slightly older and younger Ordovician biomarker studies from Gondwana, Laurentia and Baltica, particularly in relation to *G. prisca* and acritarch (sterane) assemblages. As mentioned in section 5.3, variations in carbon isotopic signatures are observed in the *G. prisca* biomass from Australia (Canning and Amadeus basins) and North America. In the Amadeus Basin, *G. prisca*-rich sediments are present in the older Lower Ordovician Horn Valley Siltstone (see e.g. McKirdy, 1977; Gorter, 1984; Elphinstone, 1989; Summons and Powell, 1991; Summons et al., 2002; Haines and Wingate, 2007). Middle Cambrian *G. prisca*-rich sediments are also known from the adjacent Georgina

Basin (e.g. Boreham and Ambrose, 2007). Whether or not the Canning, Amadeus and Georgina basins were connected at any time during the Ordovician remains controversial (e.g. Haines and Wingate, 2007; Jakobsen et al., 2013). Macrofossil fauna from the Amadeus are highly endemic in comparison to the Canning and Georgina basins (Jakobsen et al., 2013a, 2013b) and these latter basins lack the characteristic peri-Gondwanan Ordovician acritarchs (Molyneux et al., 2013). The distinctive nature of the (micro)fauna in the intracratonic Australian basins might suggest limited interaction with the open ocean because oceanic circulation patterns are thought to be reasonably well established during the Middle Ordovician (Servais et al., 2014). Results of this study show some isotopic similarities in *G. prisca* related sediments and oils of the Canning and Amadeus basins, but further work is required to systematically compare biomarker assemblages and evaluate regional similarities.

Upper Ordovician sections from Laurentia and Baltica have been used to study molecular biosignatures preserved in low latitudinal tropical environments (Pancost et al., 2013, 1999, 1998; Rohrssen et al., 2013; Mustafa et al., 2015). The Upper Ordovician (Katian–Hirnantian) in eastern Canada (Vauréal Fm. and Ellis Bay Fm.) experienced similarly high bacterial and methanotrophic activity (Rohrssen et al., 2013) as presented here for Unit 4 of the Middle Ordovician Goldwyer Formation. Both the Canadian and Australian sedimentary sections were deposited on tropical carbonate platforms. Hence, elevated bacterial and methanotrophic activity could have been a widespread phenomenon occurring throughout the Middle–Late Ordovician, as carbonate-rich shallow marine environments represented much of the epeiric seas that covered large areas of the landmasses. The sedimentary sections of eastern Canada and the Australian Goldwyer Formation show significant affiliations in chitinozoan assemblages, but this similarity is not mirrored by the associated acritarchs (Quintavalle and Playford, 2006a,b). The upper Goldwyer Formation contains higher abundances of C_{30} steranes (up to 3.1 %) in comparison to the Ordovician

localities from Canada and North America (up to 1.2%; Rohrssen et al., 2015). Differences are also noted in the C_{27}:C_{28}:C_{29} sterane distribution, with the Canadian sections showing a consistent predominance of C_{29} steranes (>60%). Furthermore, no *G. prisca* biomarker signatures are present in rock extracts from the Vauréal and Ellis Bay formations (Rohrssen et al., 2013). Although eastern Canada was situated at low latitudes during the Late Ordovician, sea surface temperatures are estimated to be more than 5 degrees cooler in comparison to the Darriwilian (Trotter et al., 2008) which may have driven the observed variations in biodiversity, both on the macrofossil and molecular scale.

Further variations are noted in sterane assemblages from other localities in Laurentia and Baltica. In Iowa and Ontario, Middle–Upper Ordovician sections exhibit either equal amounts of the C_{27} and C_{29} steranes, or a predominance of the C_{29} steranes (ca. 50–60%) (Obermajer et al., 1999; Pancost et al., 2013). In sections from Baltica, a predominance of C_{29} steranes is observed during the Katian, which shifts to a strong predominance of C_{27} steranes (ca. 50–98%) during the Hirnantian (Mustafa et al., 2015; Smolarek et al., 2017). Despite the limited amount of data, these geographical and temporal variations highlight the potential for biomarker studies to evaluate biodiversity changes throughout the Ordovician.

There is a growing body of evidence that terrestrial life originated on the Gondwanan palaeocontinent during the Early–Middle Ordovician (Steemans et al., 2010 and references therein; Edwards et al., 2014). Land-plant microfossils have been recorded from the Middle and Upper Ordovician of Gondwana and peri-Gondwana terranes (Argentina, Czech Republic, Saudi Arabia, Libya, Turkey), Avalonia and China (Steemans et al., 2010) (Fig. 13). The tetrad and dyad cryptospores from Unit 4 represent the oldest land-plant spores from Australia. They are time-equivalent to those found in other Gondwanan localities, contributing to the numerous lines of evidence that terrestrial life originated on Gondwana. Some of these studies detected land-plant spores in similar depositional environments

(Strother et al., 2015), but none include published biomarker and compound-specific stable isotope analyses. In this study, the combination of biomarkers and palynology has proven successful to identify terrigenous inputs into the marine environment. Thus, biomarkers provide a powerful tool to track terrestrial signals in Early Paleozoic settings when microfossils are either scarce or absent.

6 Conclusions

This study investigated the fossil and biomarker signature of Middle Ordovician (Darriwilian) rocks in the Canning Basin of Australia, which are coeval with the GOBE. Palynological, petrographic, molecular and stable carbon ($\delta^{13}C$) isotope analyses of biomarkers have demonstrated that the upper (Unit 4) organic-rich section of the Middle Ordovician Goldwyer Formation contains a hitherto unrecognised land plant input into the marine environment. This is the oldest occurrence of land plant microfossils (cryptospores) in Australia, supporting the observation that life on land evolved on the Gondwanan palaeocontinent. Terrestrial biomarkers identified in Unit 4 include benzonaphthofurans and ^{13}C-depleted mid-chain *n*-alkanes.

Molecular redox proxies and hopane and sterane distributions reveal differences between the upper (Unit 4) and lower (Units 1+2) Goldwyer Formation, with the microbial communities changing with the redox conditions. In Unit 4, the abundance of C_{30} sterane relative to C_{27}–C_{29} steranes exceeds those typical of Ordovician rocks, which may be linked to the distinct nature of the Australian Middle Ordovician (micro)fauna and acritarch assemblages.

Methanotrophic bacteria were abundant in Unit 4 and similar assemblages have been observed in the Upper Ordovician carbonate dominated, shallow marine sediments of Laurentia, suggesting that enhanced methane cycling played an important role in tropical carbonate dominated environments during the Middle–Late Ordovician. In Unit 4 of Solanum-1, the abundance of methanotrophic bacteria (as inferred from the 3-methylhopane index) correlated with higher inputs of *G. prisca*. The depleted carbon isotopic composition of *G. prisca* biomarkers suggests a potential ecological affiliation where methanotrophic bacteria provided the carbon source for *G. prisca*. The co-occurrence of land plants and

methanotrophic bacteria within this setting may also point towards a symbiotic relationship. These findings highlight the ecological significance of methanotrophic bacteria during the Ordovician. *G. prisca* is absent in Units 1+2 and sediments rich in *G. prisca* have an irregular distribution throughout Unit 4 in the wells studied on the Broome Platform.

The results of this study provide further insight into Ordovician palaeoenvironmental conditions for both marine- and terrestrial-ecosystems. Combining biomarkers and stable carbon isotopic studies with palynology and organic petrology has enabled the investigation into the biosignatures of early land plants. This combined approach could be applied to additional Ordovician sections where microfossils are scarce, and could assist with the delineation of the geographical distribution and origin of early land plants.

Acknowledgements

Geoff Chidlow, Peter Hopper and Alex Holman are thanked for their technical support with GC-MS and GC-irMS analyses at Curtin University. GS acknowledges Curtin University for an International Postgraduate Research Scholarship (CIPRS) and The Institute for Geoscience Reseach (TIGeR) and CSIRO for top-up scholarships. KG acknowledges the ARC for a DORA (DP130100577) grant to support this research and PhD stipend of GS. DE publishes with the permission of the CEO, Geoscience Australia. GS wishes to thank GSWA and Finder Exploration Pty Ltd for access to drill core and Leon Normore (GSWA) for his assistance with sampling. Furthermore Finder Exploration is thanked for generously providing additional data on Theia-1, including geochemical analyses performed at the Weatherford Labs. Zhongsheng Li is thanked for his contributions to the organic petrology. Carolyn L. K. Colonero assisted with MRM analyses at MIT where research was supported by an award from the Simons Foundation. Chris Elders is acknowledged for his inputs regarding geological interpretations. Chris Boreham and Takehiko (Riko) Hashimoto are thanked for their suggestions on early drafts of the manuscript. Two anonymous reviewers are thanked for their constructive and useful comments.

References

Bird, M.I., Summons, R.E., Gagan, M.K., Roksandic, Z., Dowling, L., Head, J., Fifield, L.K., Cresswell, R.G., Johnson, D.P., 1995. Terrestrial vegetation change inferred from *n*-alkane $\delta^{13}C$ analysis in the marine environment. Geochimica et Cosmochimica Acta 59, 2853–2857.

Blokker, P., van Bergen, P., Pancost, R., Collinson, M.E., de Leeuw, J.W., Sinninghe Damsté, J.S., 2001. The chemical structure of *Gloeocapsomorpha prisca* microfossils: implications for their origin. Geochimica et Cosmochimica Acta 65, 885–900.

Boreham, C.J., Ambrose, G.J., 2007. Cambrian petroleum systems in the southern Georgina

Basin, Northern Territory, Australia., in: Munson, T.J., Ambrose, G.J. (Eds), Proceedings of the Central Australian Basins Symposium (CABS), Alice Springs, Northern Territory, Northern Territory Geological Survey Special Publication 2. http://www.nt.gov.au/d/Minerals_Energy/Geoscience/Cabs/papers/P04_Boreham_Ambrose.pdf

Brader, A. V, van Winden, J.F., Bohncke, S.J.P., Beets, C.J., Reichart, G., de Leeuw, J.W., 2010. Fractionation of hydrogen , oxygen and carbon isotopes in *n*-alkanes and cellulose of three *Sphagnum* species. Organic Geochemistry 41, 1277–1284. doi:10.1016/j.orggeochem.2010.09.006

Brocks, J.J., Summons, R.E., 2014. Sedimentary hydrocarbons, biomarkers for early life, in: Holland, H., Turekian, K. (Eds.), Treatise on Geochemistry 2nd Edition. Elsevier, pp. 63–115. doi:10.1016/B978-0-08-095975-7.00803-2

Brocks, J.J., Buick, R., Logan, G.A., Summons, R.E., 2003. Composition and syngeneity of molecular fossils from the 2.78 to 2.45 billion-year-old Mount Bruce Supergroup, Pilbara Craton, Western Australia. Geochimica et Cosmochimica Acta 67, 22, 4289–4319.

Chikaraishi, Y., Naraoka, H., 2003. Compound-specific $\delta D - \delta^{13}C$ analyses of *n*-alkanes extracted from terrestrial and aquatic plants. Phytochemistry 63, 361–371. doi:10.1016/S0031-9422(02)00749-5

Cooper, R.A., Sadler, P.M., 2004. The Ordovician Period, in: A Geologic Time Scale. pp. 165–187.

Didyk, B.M., Simoneit, B.R.T., Brassell, S.C., Eglinton, G., 1978. Organic geochemical indicators of palaeoenvironmental conditions of sedimentation. Nature 272, 216–222. doi:10.1038/272216a0

Dutta, S., Brocke, R., Hartkopf-Fröder, C., Littke, R., Wilkes, H., Mann, U., 2007. Highly

aromatic character of biogeomacromolecules in Chitinozoa: a spectroscopic and pyrolytic study. Organic Geochemistry 38, 1625–1642. doi:10.1016/j.orggeochem.2007.06.014

Edwards, D., Morris, J.L., Richardson, J.B., Kendrick, P., 2014. Cryptospores and cryptophytes reveal hidden diversity in early land floras. New Phytologist 202: 50–78. doi: 10.1111/nph.12645

Edwards, D.S., Boreham, C.J., Chen, J., Grosjean, E., Mory, A.J., Sohn, J., Zumberge, J.E., 2013. Stable carbon and hydrogen isotopic compositions of Paleozoic marine crude oils from the Canning Basin: comparison with other west Australian crude oils, in: Keep, M. and Moss, S. (Eds), The Sedimentary Basins of West Australia IV. Proceedings of the Petroleum Exploration Society of Australia Symposium, Perth, 2013, pp. 1–13.

Edwards, D.S., Zumberge, J.E., 2005. The Oils of Western Australia. II. Regional Petroleum Geochemistry and Correlation of Crude Oils and Condensates from Western Australia and Papua New Guinea, Geoscience Australia and GeoMark Research Ltd unpublished report, Canberra and Houston, GEOCAT 37512, http://www.ga.gov.au/metadata-gateway/metadata/record/gcat_a05f7892-cafb-7506-e044-00144fdd4fa6/The+Oils+of+Western+Australia+II.

Edwards, D.S., Summons, R.E., Kennard, J.M., Nicoll, R.S., Bradshaw, J., Bradshaw, M.T., Foster, C.B., O'Brien, G.W., Zumberge, J.E., 1997. Geochemical characteristics of Palaeozoic petroleum systems in northwestern Australia. APPEA Journal 37(1), 351–379. doi:10.1007/PL00007202

Edwards, D.S., Murray, A.P., Foster, C.B., 1995. Hydrocarbon Composition of Carribuddy Group Sediments, Oils and Bitumens from the Admiral Bay Fault Zone, Canning Basin. Australian Geological Survey Organisation, 31p. DAR 1427

Eglinton, G., Hamilton, R.J., 1967. Leaf epicuticular waxes. Science 156, 1322–1335.

Eley, Y., Dawson, L., Pedentchouk, N., 2016. Investigating the carbon isotope composition and leaf wax n-alkane concentration of C3 and C4 plants in Stiffkey saltmarsh, Norfolk, UK. Organic Geochemistry 96, 28–42. doi:10.1016/j.orggeochem.2016.03.005

Elphinstone R., 1989. Sedimentology and facies distribution within the Horn Valley Siltstone, Amadeus Basin: a reconnaissance study. Bureau of Mineral Resources, Australia, Record 1992/02. http://www.ga.gov.au/metadata-gateway/metadata/record/gcat_a05f7892-759f-7506-e044-00144fdd4fa6/Sedimentology+and+Facies+Distribution+within+the+Horn+Valley+Siltstone%2C+Amadeus+Basin+%3A+A+Reconnaissance+Study

Farrimond, P., Talbot, H.M., Watson, D.F., Schulz, L.K., Wilhelms, A., 2004. Methylhopanoids: molecular indicators of ancient bacteria and a petroleum correlation tool. Geochimica et Cosmochimica Acta 68, 3873–3882. doi:10.1016/j.gca.2004.04.011

Fensome, R.A., MacRae, R.A., Moldowan, J.M., Taylor, F.J.R., Williams, G.L. 1996. The early Mesozoic radiation of dinoflagellates. Paleobiology 22, 3, 329–338.

Ficken, K.J., Li, B., Swain, D.L., Eglinton, G., 2000. An *n*-alkane proxy for the sedimentary input of submerged/floating freshwater aquatic macrophytes. Organic Geochemistry 31, 745–749. doi:10.1016/S0146-6380(00)00081-4

Finder Exploration Pty Ltd, 2015. Theia 1 Rig Release and Cessation of Operations, 31 August 2015. http://www.finderexp.com/wp-content/uploads/2015/08/Cessation%20of%20operations%20at%20Theia-1%2031%20Aug%2015.pdf.

Forman, D.J., Wales, D.W., 1981. Geological evolution of the Canning Basin, Western Australia. Bureau of Mineral Resources Bulletin 210, 1–390.

Foster, C.B., O'Brien, G.W., Watson, S.T., 1986. Hydrocarbon source potential of the Goldwyer Formation, Barbwire Terrace, Canning Basin, Western Australia. APEA

Journal 26, 142–155.

Foster, C., Reed, J., Wicander, R., 1989. *Gloeocapsomorpha prisca* Zalessky 1917: A new study part 1: taxonomy, geochemistry and paleoecology. Geobios 22, 735–759.

Foster, C.B., Wicander, R., Reed, J., 1990. *Gloeocapsomorpha prisca* Zalessky, 1917: A new study part II: origin of kukersite, a new interpretation. Geobios 23, 133–140.

Fowler, M.G., Stasiuk, L.D., Hearn, M., Obermajer, M., 2004. Evidence for *Gloeocapsomorpha prisca* in Late Devonian source rocks from Southern Alberta, Canada. Organic Geochemistry 35, 425–441. doi:10.1016/j.orggeochem.2004.01.017

Gill, B.C., Lyons, T.W., Saltzman, M.R., 2007. Parallel, high-resolution carbon and sulfur isotope records of the evolving Paleozoic marine sulfur reservoir. Palaeogeography, Palaeoclimatology, Palaeoecology 256, 156–173. doi:10.1016/j.palaeo.2007.02.030

Gorter, J.D., 1984. Source potential of the Horn Valley Siltstone, Amadeus Basin. APEA Journal, 24(1): 66-91.

Grantham, P.J., Wakefield, L.L., 1988. Variations in the sterane carbon number distributions of marine source rock derived crude oils through geological time. Organic Geochemistry 12, 1, 61–73.

Grice, K., Cao, C., Love, G.D., Bottcher, M.E., Twitchett, R., Grosjean, E., Summons, R.E., Turgeon, S.E., Dunning, W., Jin, Y., 2005. Photic zone euxinia during the Permian-Triassic superanoxic event. Science 307, 706–709.

Grice, K., Schaeffer, P., Schwark, L., Maxwell, J.R., 1996. Molecular indicators of palaeoenvironmental conditions in an immature Permian shale (Kupferschiefer, Lower Rhine Basin, north-west Germany) from free and S-bound lipids. Organic Geochemistry 25, 3/4, 131–147.

Grosjean, E., Love, G.D., Stalvies, C., Fike, D.A., Summons, R.E., 2009. Origin of petroleum in the Neoproterozoic-Cambrian South Oman Salt Basin. Organic Geochemistry 40, 87–

110. doi:10.1016/j.orggeochem.2008.09.011

Gupta, N.S., Briggs, D.E., Pancost, R.E., 2006. Molecular taphonomy of graptolites. Journal of the Geological Society London 163, 897–900.

Guthrie, J.M., Pratt, L.M., 1995. Geochemical character and origin of oils in Ordovician reservoir rocks, Illinois and Indiana, USA. American Association of Petroleum Geologists Bulletin 79, 1631–1649. doi:10.1306/7834DE36-1721-11D7-8645000102C1865D

Haines, P.W., Wingate, M.T.D., 2007. Contrasting depositional histories, detrital zircon provenance and hydrocarbon systems: did the Larapintine seaway link the Canning and Amadeus Basin during the Ordovician? Proceedings Central Australian Basin Symposium, Special Publications 2, 36–51.

Haines, P.W., 2004. Depositional facies and regional correlation for the Ordovician Goldwyer and Nita formations Canning Basin, Western Australia with implications for petroleum exploration: Western Australia Geological Survey, Record 2004/7, 45p.

Hammarlund, E.U., Dahl, T.W., Harper, D.A.T., Bond, D.P.G., Nielsen, A.T., Bjerrum, C.J., Schovsbo, N.H., Schönlaub, H.P., Zalasiewicz, J.A., Canfield, D.E., 2012. A sulfidic driver for the end-Ordovician mass extinction. Earth and Planetary Science Letters 331–332, 128–139. doi:10.1016/j.epsl.2012.02.024

Harper, D.A.T., 2006. The Ordovician biodiversification: setting an agenda for marine life. Palaeogeography, Palaeoclimatology, Palaeoecology 232, 148–166. doi:10.1016/j.palaeo.2005.07.010

Hartkopf-Fröder, C., Königshof, Littke, R. and Schwarzbauer, J., 2015. Optical thermal maturity parameters and organic geochemical alteration at low grade diagenesis to anchimetamorphism: A review. International Journal of Coal Geology, 151-152, 74-119.

Hoffmann, C.F., Foster, C.B., Powell, T.G., Summons, R.E., 1987. Hydrocarbon biomarkers

from Ordovician sediments and the fossil alga *Gloeocapsomorpha prisca* Zalessky 1917. Geochimica et Cosmochimica Acta 51, 2681–2697. doi:10.1016/0016-7037(87)90149-9

Hughes, W.B., Holba, A.G., Dzou, L.I.P., 1995. The ratios of dibenzothiophene to phenanthrene and pristane to phytane as indicators of depositional environment and lithology of petroleum source rocks. Geochimica et Cosmochimica Acta 59, 3581–3598. doi:10.1016/0016-7037(95)00225-O

Inglis, G.N., Collinson, M.E., Riegel, W., Wilde, V., Robson, B.E., Lenz, O.K., Pancost, R.D., 2015. Ecological and biogeochemical change in an early Paleogene peat-forming environment: linking biomarkers and palynology. Palaeogeography, Palaeoclimatology, Palaeoecology 438, 245–255. doi:10.1016/j.palaeo.2015.08.001

Jacob, J., Paris, F., Monod, O., Miller, M.A., Tang, P., George, S.C., Bény, J., 2007. New insights into the chemical composition of chitinozoans. Organic Geochemistry 38, 1782–1788.

Jarrett, A., Edwards, D.S., Boreham, C., McKirdy, D.M., 2016. Petroleum geochemistry of the Amadeus Basin. AGES 2016 Conference Proceedings, NT Geological Survey. http://geoscience.nt.gov.au/gemis/ntgsjspui/handle/1/82725

Kennard, J.M., Jackson, M.J., Romine, K.K., Shaw, R.D., Southgate, P.N., 1994. Depositional sequences and associated petroleum systems of the Canning Basin, WA, in: Purcell, P.G. and Purcell, R.R. (Eds), The Sedimentary Basins of Western Australia. Proceedings of the Petroleum Exploration Society of Australia Symposium, Perth, WA, pp. 658–676.

Kiipli, E., Kiipli, T., 2013. Nitrogen isotopes in kukersite and black shale implying Ordovician-Silurian seawater redox conditions. Oil Shale 30, 60–75. doi:10.3176/oil.2013.1.06

Kip, N., van Winden, J.F., Pan, Y., Bodrossy, L., Reichart, G.-J., Smolders, A.J.P., Jetten, M.S.M., Sinninghe Damsté, J.S., Op den Camp, H.J.M., 2010. Global prevalence of methane oxidation by symbiotic bacteria in peat-moss ecosystems. Nature Geoscience 3, 617–621. doi:10.1038/ngeo939

Koopmans, M.P., Köster, J., van Kaam-Peters, H.M.E., Kenig, F., Schouten, S., Hartgers, W.A., De Leeuw, J.W., Sinninghe Damsté, J.S., 1996. Diagenetic and catagenetic products of isorenieratene: molecular indicators for photic zone anoxia. Geochimica et Cosmochimica Acta 60, 4467–4496. doi:10.1016/S0016-7037(96)00238-4

LaPorte, D.F., Holmden, C., Patterson, W.P., Loxton, J.D., Melchin, M.J., Mitchell, C.E., Finney, S.C., Sheets, H.D., 2009. Local and global perspectives on carbon and nitrogen cycling during the Hirnantian glaciation. Palaeogeography, Palaeoclimatology, Palaeoecology 276, 182–195. doi:10.1016/j.palaeo.2009.03.009

Le Heron, D.P., Craig, J., Etienne, J.L., 2009. Ancient glaciations and hydrocarbon accumulations in North Africa and the Middle East. Earth-Science Reviews 93, 47–76. doi:10.1016/j.earscirev.2009.02.001

Lenton, T.M., Crouch, M., Johnson, M., Pires, N., Dolan, L., 2012. First plants cooled the Ordovician. Nature Geoscience 5, 86–89. doi:10.1038/ngeo1390

Lenton, T.M., Dahl, T.W., Daines, S.J., Mills, B.J.W., Ozaki, K., Saltzman, M.R., Porada, P., 2016. Earliest land plants created modern levels of atmospheric oxygen. Proceedings of the National Academy of Sciences 113, 9704–9709. doi:10.1073/pnas.1604787113

Li, M., Ellis, G.S., 2015. Qualitative and quantitative analysis of dibenzofuran, alkyldibenzofurans, and benzo[*b*]naphthofurans in crude oils and source rock extracts. Energy & Fuels 29, 1421–1430. doi:10.1021/ef502558a

Luo, G., Algeo, T.J., Zhan, R., Yan, D., Huang, J., Liu, J., Xie, S., 2016. Perturbation of the marine nitrogen cycle during the Late Ordovician glaciation and mass extinction.

Palaeogeography, Palaeoclimatology, Palaeoecology 448, 339–348. doi:10.1016/j.palaeo.2015.07.018

McKirdy, D.M., 1977. Diagenesis of microbial organic matter, PhD thesis, Australian National University, Canberra.

McKirdy, D.M., Thorpe, C.S., Haynes, D.E., Grice, K., Krull, E.S., Halverson, G.P., Webster, L.J., 2010. The biogeochemical evolution of the Coorong during the mid- to late Holocene: an elemental, isotopic and biomarker perspective. Organic Geochemistry 41, 96–110. doi:10.1016/j.orggeochem.2009.07.010

Mead, R., Xu, Y., Chong, J., Jaffle, R., 2005. Sediment and soil organic matter source assessment as revealed by the molecular distribution and carbon isotopic composition of *n*-alkanes. Organic Geochemistry 36, 363–370.

Melchin, M.J., Mitchell, C.E., Holmden, C., Štorch, P., 2013. Environmental changes in the Late Ordovician – early Silurian : review and new insights from black shales and nitrogen isotopes. GSA Bulletin 125, 1635–1670. doi:10.1130/B30812.1

Moldowan, J.M., Seifert, W.K., Gallegos, E.J., 1985. Relationship between petroleum composition and depositional environment of petroleum source rocks. The American Association of Petroleum Geologists Bulletin 16, 191–207. doi:10.1080/10916469808949779

Moldowan, J.M., Fago, F.J., Lee, C.Y., Jacobson, S.R., Watt, D.S., Slougui, N., Jeganathan, A., Young, D.C., 1990. Sedimentary 24-*n*-propylcholestanes, molecular fossils diagnostic of marine algae. Science 247, 309–312.

Moldowan, J.M., Talyzina, N.M., 1998. Biogeochemical evidence for dinoflagellate ancestors in the Early Cambrian. Science 281, 1168–1170. doi: 10.1126/science.281.5380.1168

Molyneux, S.G., Delabroye, A., Wicander, R., Servais, T., 2013. Biogeography of early to

mid Palaeozoic (Cambrian–Devonian) marine phytoplankton. Geological Society Memoir 38, 1, 365–397.

Munnecke, A., Calner, M., Harper, D.A.T., Servais, T., 2010. Ordovician and Silurian sea-water chemistry, sea level, and climate: a synopsis. Palaeogeography, Palaeoclimatology, Palaeoecology 296, 389–413. doi:10.1016/j.palaeo.2010.08.001

Mustafa, K.A., Sephton, M.A., Watson, J.S., Spathopoulos, F., Krzywiec, P., 2015. Organic geochemical characteristics of black shales across the Ordovician-Silurian boundary in the Holy Cross Mountains, central Poland. Marine and Petroleum Geology 66, 1042–1055. doi:10.1016/j.marpetgeo.2015.08.018

Naraoka, H., Ishiwatari, R., 1999. Carbon isotopic compositions of individual long-chain *n*-fatty acids and *n*-alkanes from river to open ocean: multiple origins for their occurrence. Geochemical Journal 33, 215–235.

Nichols, J.E., Isles, P.D.F., Peteet, D.M., 2014. A novel framework for quantifying past methane recycling by *Sphagnum*-methanotroph symbiosis using carbon and hydrogen isotope ratios of leaf wax biomarkers. Geochemistry, Geophysics, Geosystems 15, 1827–1836. doi:10.1002/2014GC005242

Obermajer, M., Fowler, M.G., Snowdon, L.R., 1999. Depositional environment and oil generation in Ordovician source rocks from southwestern Ontario, Canada: organic geochemical and petrological approach. AAPG Bulletin 83, 1426–1453. doi:10.1306/E4FD41D9-1732-11D7-8645000102C1865D

Otto, A., Simoneit, B.R.T., 2001. Chemosystematics and diagenesis of terpenoids in fossil conifer species and sediment from the Eocene Zeitz Formation, Saxony, Germany. Geochimica et Cosmochimica Acta 65, 3505–3527. doi:10.1016/S0016-7037(01)00693-7

Pancost, R.D., Freeman, K.H., Herrmann, A.D., Patzkowsky, M.E., Ainsaar, L., Martma, T.,

2013. Reconstructing Late Ordovician carbon cycle variations. Geochimica et Cosmochimica Acta 105, 433–454. doi:10.1016/j.gca.2012.11.033

Pancost, R.D., Freeman, K.H., Patzkowsky, M.E., 1999. Organic-matter source variation and the expression of a late Middle Ordovician carbon isotope excursion. Geology 27, 1015–1018. doi:10.1130/0091-7613(1999)027<1015:OMSVAT>2.3.CO

Pancost, R.D., Freeman, K.H., Patzkowsky, M.E., Wavrek, D.A., Collister, J.W., 1998. Molecular indicators of redox and marine photoautotroph composition in the late Middle Ordovician of Iowa, U.S.A. Organic Geochemistry 29, 1649–1662. doi:10.1016/S0146-6380(98)00185-5

Peters, K.E., Walters, C.C., Moldowan, J.M., 2005. The Biomarker Guide Volume 2. Biomarkers and Isotopes in Petroleum Systems and Earth History, 2nd ed. Cambridge University Press.

Quintavalle, M., Playford, G., 2008. Stratigraphic distribution of selected acritarchs in the Ordovician subsurface, Canning Basin, Western Australia. Revue de micropaléontologie 51, 23-37. doi:10.1016/j.revmic.2006.11.003

Quintavalle, M., Playford, G., 2006a. Palynostratigraphy of Ordovician strata, Canning Basin, Western Australia. Part One: acritarchs and prasinophytes. Palaeontographica Abteilung B: 275(1-3), 1-88.

Quintavalle, M., Playford, G., 2006b. Palynostratigraphy of Ordovician strata, Canning Basin, Western Australia. Part Two: chitinozoans and biostratigraphy. Palaeontographica Abteilung B: 275(4-6), 89-131.

Redecker, D., Kodner, R., Graham, L.E., 2000. Glomalean fungi from the Ordovician. Science 289, 1920–1921.

Reed, J.D., Illich, H.A., Horsfield, B., 1986. Biochemical evolutionary significance of Ordovician oils and their sources. Organic Geochemistry 10, 347–358.

doi:10.1016/0146-6380(86)90035-5

Ricci, J.N., Michel, A.J., Newman, K., 2015. Phylogenetic analysis of HpnP reveals the origin of 2-methylhopanoid production in Alphaproteobacteria. Geobiology 13, 267–277.

Ricci, J.N., Coleman, M.L., Welander, P. V, Sessions, A.L., Summons, R.E., Spear, J.R., Newman, D.K., 2014. Diverse capacity for 2-methylhopanoid production correlates with a specific ecological niche. International Society for Microbial Ecology 8, 675–684. doi:10.1038/ismej.2013.191

Rieley, G., Collier, R.J., Jones, D.M., Eglinton, G., Eakin, P.A., Fallick, A.E., 1991. Sources of sedimentary lipids deduced from stable carbon-isotope analyses of individual compounds. Nature 352, 425–427.

Rohrssen, M., Gill, B.C., Love, G.D., 2015. Scarcity of the C_{30} sterane biomarker, 24-*n*-propylcholestane, in Lower Paleozoic marine paleoenvironments. Organic Geochemistry 80, 1-7. doi:10.1016/j.orggeochem.2014.11.008

Rohrssen, M., Love, G.D., Fischer, W., Finnegan, S., Fike, D.A., 2013. Lipid biomarkers record fundamental changes in the microbial community structure of tropical seas during the Late Ordovician Hirnantian glaciation. Geology 41, 127–130. doi:10.1130/G33671.1

Romero-Sarmiento, M.F., Riboulleau, A., Vecoli, M., Versteegh, G.J.M., 2011. Aliphatic and aromatic biomarkers from Gondwanan sediments of Late Ordovician to Early Devonian age: an early terrestrialization approach. Organic Geochemistry 42, 605–617. doi:10.1016/j.orggeochem.2011.04.005

Romine, K.K., Southgate, P.N., Kennard, J.M., Jackson, M.J., 1994. The Ordovician to Silurian phase of the Canning Basin WA: structure and sequence evolution, in: Purcell, P.G. and Purcell, R.R. (Eds), The Sedimentary Basins of Western Australia. Proceedings of the Petroleum Exploration Society of Australia Symposium, Perth, 1994, pp. 677–

696.

Royles, J., Horwath, A.B., Griffiths, H., 2014. Interpreting bryophyte stable carbon isotope composition: plants as temporal and spatial climate recorders. Geochemistry, Geophysics, Geosystems 15, 1462–1475. doi:10.1002/2013GC005169.Received

Rubinstein, C.V, Gerrienne, P., de la Puente, G.S., Astini, R.A., Steemans, P., 2010. Early Middle Ordovician evidence for land plants in Argentina (eastern Gondwana). New Phytologist 188, 365–369. doi:10.1111/j.1469-8137.2010.03433.x

Schoenherr, J., Littke, R., Urai, J.L., Kukla, P.A., Rawahi, Z., 2007. Polyphase thermal evolution in the Infra-Cambrian Ara Group (South Oman Salt Basin) as deducted by maturity of solid reservoir bitumen, Organic Geochemistry, 38, 1293-1318.

Schwark, L., Empt, P., 2006. Sterane biomarkers as indicators of palaeozoic algal evolution and extinction events. Palaeogeography, Palaeoclimatology, Palaeoecology 240, 225–236.

Schwark, L., Frimmel, A., 2004. Chemostratigraphy of the Posidonia Black Shale, SW-Germany II. Assessment of extent and persistence of photic-zone anoxia using aryl isoprenoid distributions, Chemical Geology 206, 231–248. doi:10.1016/j.chemgeo.2003.12.008

Sephton, M.A., van Looy, C., Brinkhuis, H., Wignall, P.B., de Leeuw, J., Visscher, H., 2005. Catastrophic soil erosion during the end-Permian biotic crisis. Geology 33, 941–944. doi:10.1130/G21784.1

Servais, T., Harper, D.A.T., Li, J., Munnecke, A., Owen, A.W., Sheehan, P.M., 2009. Understanding the Great Ordovician Biodiversification Event (GOBE): influences of paleogeography, paleoclimate, or paleoecology? GSA Today 19, 4–10. doi:10.1130/GSATG37A.1

Servais, T., Li, J., Molyneux, S., Raevskaya, E., 2003. Ordovician organic-walled

microphytoplankton (acritarch) distribution: the global scenario. Palaeogeography, Palaeoclimatology, Palaeoecology 195, 149-172. doi:10.1016/S0031-0182(03)00306-7

Sherwood, N., Li, Z., 2016. Source rock evaluation using vitrinite reflectance and maceral analyses for a suite of rocks sampled from various wells drilled in the Canning Basin, Western Australia and the Amadeus Basin, Northern Territory, Australia. Geoscience Australia, Resources Division Report 2016/00.

Sinninghe Damsté, J.S., Kenig, F., Koopmans, M.P., Koster, J., Schouten, S., Hayes, J.M., de Leeuw, J.W., 1995. Evidence for gammacerane as an indicator of water column stratification. Geochimica et Cosmochimica Acta 59, 1895–1900. doi:10.1016/0016-7037(95)00073-9

Smolarek, J., Marynowski, L., Trela, W., Kujawski, P., Simoneit, B. 2017. Redox conditions and marine microbial community changes during the end-Ordovician mass extinction event. Global and Planetary Change 149, 105-122. http://dx.doi.org/10.1016/j.gloplacha.2017.01.002

Steemans, P., Hérissé, A. Le, Melvin, J., Miller, M.A., Paris, F., Verniers, J., Wellman, C.H., 2009. Origin and radiation of the earliest vascular land plants. Science 324, 353. doi:10.1126/science.1169659

Steemans, P., Wellman, C.H., Gerrienne, P., 2010. Palaeogeographic and palaeoclimatic considerations based on Ordovician to Lochkovian vegetation. Geological Society London Special Publications 339, 49–58. doi:10.1144/SP339.5

Strother, P.K., Traverse, A., Vecoli, M., 2015. Cryptospores from the Hanadir Shale Member of the Qasim Formation, Ordovician (Darriwilian) of Saudi Arabia: taxonomy and systematics. Review of Palaeobotany and Palynology 212, 97–110. doi:10.1016/j.revpalbo.2014.08.018

Summons, R.E., Bradley, A.S., Jahnke, L.L., Waldbauer, J.R., 2006. Steroids, triterpenoids

and molecular oxygen. Philosophical Transactions of the Royal Society B: Biological Sciences 361, 951–968. doi:10.1098/rstb.2006.1837

Summons, R.E., Zumberge, J.E., Boreham, C.J., Bradshaw, M.T., Brown, S.W., Edwards, D.S., Hope, J., Johns, N., 2002. The Oils of Eastern Australia: petroleum geochemistry and correlation. GeoMark and Geoscience Australia. Volume 2. https://ecat.ga.gov.au/geonetwork/srv/eng/search#!a05f7892-ff6d-7506-e044-00144fdd4fa6

Summons, R.E., Jahnke, L.L., Hope, J.M., Logan, G. A, 1999. 2-Methylhopanoids as biomarkers for cyanobacterial oxygenic photosynthesis. Nature 400, 554–557. doi:10.1038/23005

Summons, R.E., Jahnke, L.L., Roksandic, Z., 1994. Carbon isotopic fractionation in lipids from methanotrophic bacteria: relevance for interpretation of the geochemical record of biomarkers. Geochimica et Cosmochimica Acta 58, 2853–2863. doi:10.1016/0016-7037(94)90119-8

Summons, R. E., Powell, T.G., 1991. Petroleum source rocks of the Amadeus Basin. Geological and Geophysical Studies in the Amadeus Basin, Central Australia. K.R.J. and J.M. Kennard. Bureau of Mineral Resources, Canberra. Bulletin 236: 511-524.

Summons, R.E., Jahnke, L.L., 1990. Identification of the methylhopanes in sediments and petroleum. Geochimica et Cosmochimica Aacta 54, 247–251. doi:10.1016/0016-7037(90)90212-4

Summons, R.E., Powell, T.G., 1987. Identification of aryl isoprenoids in source rocks and crude oils: Biological markers for the green sulphur bacteria. Geochimica et Cosmochimica Acta 51, 557–566.

Talyzina, N.M., Moldowan, J.M., Johannisson, A., Fago, F.J., 2000. Affinities of Early Cambrian acritarchs studied by using microscopy, fluorescence flow cytometry and

biomarkers. Review of Palaeobotany and Palynology 108, 37–53. doi:10.1016/S0034-6667(99)00032-9

Thompson, C.K., Kah, L.C., 2012. Sulfur isotope evidence for widespread euxinia and a fluctuating oxycline in Early to Middle Ordovician greenhouse oceans. Palaeogeography, Palaeoclimatology, Palaeoecology 313–314, 189–214. doi:10.1016/j.palaeo.2011.10.020

Trabucho-Alexandre, J., Hay, W.W., de Boer, P.L., 2011. Phanerozoic environments of black shale deposition and the Wilson Cycle. Solid Earth Discussions 3, 743–768. doi:10.5194/se-3-29-2012

Triche, N.E., Bahar, M., 2013. Shale gas volumetrics of unconventional resource plays in the Canning Basin, Western Australia, in: SPE Unconventional Resources Conference and Exhibition Asia Pacific, Brisbane, Australia, 11-13 November 2013.

Tulipani, S., Grice, K., Krull, E., Greenwood, P., Revill, A.T., 2014. Salinity variations in the northern Coorong Lagoon, South Australia: significant changes in the ecosystem following human alteration to the natural water regime. Organic Geochemistry 75, 74–86. doi:10.1016/j.orggeochem.2014.04.013

Tulipani, S., Grice, K., Greenwood, P.F., Schwark, L., Böttcher, M.E., Summons, R.E., Foster, C.B., 2015. Molecular proxies as indicators of freshwater incursion-driven salinity stratification. Chemical Geology 409, 61–68. doi:10.1016/j.chemgeo.2015.05.009

van Aarssen, B.G.K., Alexander, R., Kagi, R.I., 2000. Higher plant biomarkers reflect palaeovegetation changes during Jurassic times. Geochimica et Cosmochimica Acta 64, 1417–1424.

Vandenbroucke, T.R.A., Armstrong, H.A., Williams, M., Zalasiewicz, J.A., Sabbe, K., 2009. Ground-truthing Late Ordovician climate models using the paleobiogeography of

graptolites. Paleoceanography 24, 1–19. doi:10.1029/2008PA001720

Versteegh, G.J.M., Riboulleau, A., 2010. An organic geochemical perspective on terrestrialization. Geological Society London Special Publications 339, 11–36. doi:10.1144/SP339.3

Volkman, J.K., 2006. Lipid markers for marine organic matter, in: Handbook of Environmental Chemistry, Volume 2: Reactions and Processes. pp. 27–70. doi:10.1007/698_2_002

Volkman, J.K., 1986. A review of sterol markers for marine and terrigenous organic matter. Organic Geochemistry 9, 83–99. doi:10.1016/0146-6380(86)90089-6

Wang, S., Liu, S., Lin, Z., Li, R., Wang, X., Zhou, C., Lou, H., Wang, S., Liu, S., Lin, Z., Li, R., Wang, X., 2013. Terpenoids from the Chinese liverwort *Plagiochila pulcherrima* and their cytotoxic effects. Journal of Asian Natural Products Research 15, 473–481. doi:10.1080/10286020.2013.785529

Welander, P. V., Summons, R.E., 2012. Discovery, taxonomic distribution, and phenotypic characterization of a gene required for 3-methylhopanoid production. Proceedings of the National Academy of Sciences 109, 12905–12910. doi:10.1073/pnas.1208255109

Wellman, C.H., Gray, J., 2000. The microfossil record of early land plants. Philosophical Transactions of the Royal Society B: Biological Sciences 355, 717–732.

Winchester-Seeto, T., Foster, C., O'Leary, T., 2000. Chitinozoans from the Middle Ordovician (Darriwilian) Goldwyer and Nita formations, Canning Basin (Western Australia). Acta Palaeontologica Polonica 45, 271–300.

Wright, N., Zahirovic, S., Müller, R.D., Seton, M., 2013. Towards community-driven paleogeographic reconstructions: integrating open-access paleogeographic and paleobiology data with plate tectonics. Biogeosciences 10, 1529-1541. doi:10.5194/bg-10-1529-2013

Captions of tables and figures

Table 1: Summary of Rock-Eval pyrolysis, biomarker and organic petrological data for Units 1+2 and Unit 4 of the Goldwyer Formation in Goldwyer-1, Solanum-1, Santalum-1A and Theia-1.

Table 2: Summary of palynomorph assemblages and key species identified in this study in the Goldwyer Formation in Goldwyer-1, Santalum1A, Solanum-1 and Theia-1.

Table 3: Key aliphatic and aromatic biomarker parameters for Units 1+2 and Unit 4 of the Goldwyer Formation in Goldwyer-1, Solanum-1, Santalum-1A and Theia-1.

Table 4: *n*-Alkane-specific $\delta^{13}C$ values [‰ VPDB] for selected samples from Units 1+2 and Unit 4 of the Goldwyer Formation in selected Canning Basin wells. Reported values represent average values of two or more measurements where the difference between the measurements was equal to, or less than, 0.5 per mil. Where there is no value, the peaks were too small to be measured reliably.

Table 5: Key aliphatic and aromatic hydrocarbon signatures identified in samples from the Goldwyer Formation and their paleobiological and/or environmental interpretation. *n*-Alkane carbon isotopic values are interpreted to signify different source inputs to Unit 4 at Solanum-1 and Santalum-1A.

Table 6: Average $\delta^{13}C$ values for short- (C_{16}–C_{19}) and mid to long- (C_{23}–C_{32}) chain *n*-alkanes in samples from the Goldwyer Formation. The *n*-alkanes show a progressive depletion with increasing carbon number, but the depletion is notably greater in Santalum-1A (Δ) in comparison to other samples.

Figure 1: Well location map and well-well correlation panel showing gamma ray logs, lithological logs, total organic carbon content and depths of the samples analysed.

Figure 2: Palynostratigraphy of the Goldwyer Formation in the Canning Basin and correlation of palynozones with Unit 1, 2, 3 and 4. Modified from Quintavalle and Playford, 2006b.

Figure 3: Photomicrographs of selected microfossils and cryptospores identified in assemblages from Unit 4. Scale bar in micrometres. (a) Scolecodont (worm jaw), Goldwyer-1, 873.9–876.6 m; (b) chitinozoan , Goldwyer-1, 873.9–876.6 m; (c) graptolite, Goldwyer-1, 873.9–876.6 m; (d) *Sacculidium aduncum* (Playford and Martin, 1984) emend. Ribecai et al. 2002, Theia-1, 1217.67–1217.7 m; (e) *Pirea* sp. cf. *P. ornata* (Burmann 1970) Eisenack et al. 1976 , Theia-1,1217.67–1217.7 m;(f) *Striatotheca indistincta* Quintavalle and Playford 2006, Theia-1, 1217.67–1217.7 m [same scale as 3e]; (g) *Gloeocapsomorpha prisca* Zalessky 1917 emend. Foster et al. 1989, Santalum-1A, 449.7–449.8 m; (h) cryptospore with what appears to be a trilete mark, Theia-1, 1217.67–1217.7 m; and (i) enclosed cryptospore tetrad, Theia-1, 1217.67–1217.7 m.

Figure 4: Photomicrographs taken under white light and, where specified, UV light using oil immersion. (a) Telalginite derived from *G. prisca* in Santalum-1A, 449.7–449.8 m, under white and UV light, (b) Telalginite derived from *G. prisca*, lamalginite and liptodetrinite in Solanum-1, 296.4–296.6 m, under UV light, (c) Telalginite derived from *G. prisca* in Solanum-1, 302.8-303.0 m under UV light, and (d) periderm layering in a graptolite in Goldwyer-1, 972.7–975.7 m.

Figure 5: Chromatograms (*m/z* 57) showing the *n*-alkane distributions in the lower (Units 1+2) and upper (Unit 4) Goldwyer Formation. (a) Solanum-1, 315.58–315.59 m, (b) Santalum-1A, 478.2–478.4 m, (c) Goldwyer-1, 873.9–876.6 m, (d) Goldwyer-1, 980.0–983.6 m, (e) Theia-1, 1271.48–1271.52 m, and (f) Theia-1, 1552.70–1552.75 m.

Figure 6: MRM transitions showing C_{30} steranes and C_{30} methylsteranes identified in selected samples. Identification based on an oil standard and Grosjean et al., (2009).

Figure 7: Relative abundances of *n*-alkanes and $\delta^{13}C$ of selected samples from Solanum-1 showing relatively depleted *n*-alkane $\delta^{13}C$ when the *G. prisca*-derived C_{15}–C_{19} OEP becomes predominant. $\delta^{13}C$ values provided in Table 4.

Figure 8: $\delta^{13}C$ values of *n*-alkanes from Solanum-1 that exhibit the C_{15}–C_{19} OEP signature against the range observed for *G. prisca*–rich bitumens from North America.

Figure 9: Relative abundances of *n*-alkanes and $\delta^{13}C$ of selected samples from Solanum-1 and Santalum-1A showing a shift towards depleted stable carbon isotopic signatures when the mid-chain *n*-alkanes are abundant. $\delta^{13}C$ values provided in Table 4.

Figure 10: Biomarker differences between the lower (Units 1+2) and upper (Unit 4) Goldwyer Formation as shown by (a) Pr/Ph versus gammacerane index, (b) Pr/Ph versus DBT/P, (c) H/St *versus* 2MeH/3MeH and (d) 3-methylhopane index (3MHI) (%) *versus* 2MeH/3MeH. MeH = methylhopane.

Figure 11: Graphical representation of the microbial community during deposition of Unit 4.

Figure 12: Depth profiles in Solanum-1 of TOC content and selected molecular parameters indicating the change in microbial communities through the upper (Unit 4) Goldwyer Formation. Dashed lines indicate the top (284m) and base (317m) of Unit 4 as reported by Haines (2009). Log of the *n*-alkanes C_{17}+C_{19} over C_{18}+C_{20} represents the odd-over-even predominance caused by a contribution of *G. prisca*. Blue = *G. prisca*-poor; Green = *G. prisca*-rich. Pr = Pristane; Ph = Phytane; MHI = methylhopane index; 3MHI = 3β-methyl C_{30} hopane/(3β-methyl C_{30} hopane + C_{30} hopane) × 100; 2MHI = 2α-methyl C_{30} hopane/(2α-methyl C_{30} hopane + C_{30} hopane) × 100; C_{30} steranes (%) = C_{30} steranes/ΣC_{27}–C_{30} steranes × 100; C_{30} methylsteranes (%) = abundance of selected methylated 24-ethylcholestanes (2α-, 3β-, 4α- and 4β-)/(ΣC_{27}–C_{29} steranes + C_{30} methylsteranes) × 100; C_{35} homohopane index = C_{35} αβ hopanes (22S+22R)/ΣC_{31}–C_{35} αβ hopanes (22S+22R) × 100. Phanerozoic

hopane/sterane average from Peters et al. (2005), Late Ordovician C_{30} sterane (%) range from Rohrssen et al. (2015).

Figure 13: Palaeogeographic reconstruction of the mid-Ordovician (452 Ma) centered around Australia after Wright et al. (2013). Stars represent localities of Early–Middle Ordovician cryptospores.

Table 1

Well	Upper Depth (m)	Lower Depth (m)	Unit	Lithology	TOC (wt. %)	HI (mg HC/g TOC)	OI (mg CO_2/g TOC)	Tmax (°C)	PI	C_{31} H (S/ S+R)	C_{29} ααα St S/(S+R)	dia St/(dia+ reg St)	MPI	Mean Faunal Reflect. (%)	Mean Bitumen Reflect. (%)
Solanum-1	280.0	280.2	4	Carbonate	0.30	16	241	421	0	0.60	0.42	0.42	n.d.	n.d.	0.41
Solanum-1	284.5	284.6	4	Carbonate	0.27	93	142	440	0	0.59	0.45	0.44	0.39	n.d.	n.d.
Solanum-1	291.6	291.8	4	Carbonate	0.26	62	146	435	0.12	0.59	0.48	0.39	0.39	n.d.	n.d.
Solanum-1	296.4	296.6	4	Carbonate	0.37	110	98	435	0.02	0.59	0.50	0.39	0.42	0.71	n.d.
Solanum-1	302.8	303.0	4	Carbonate	0.34	89	136	434	0.03	0.58	0.49	0.41	0.39	0.68	0.40
Solanum-1	304.7	304.8	4	Carbonate	0.18	158	120	436	0.07	0.63	0.54	0.50	n.d.	n.d.	n.d.
Solanum-1	308.8	308.9	4	Carbonate	0.37	435	55	439	0.03	0.59	0.54	0.46	n.d.	n.d.	n.d.
Solanum-1	310.3	310.4	4	Carbonate	0.1	129	230	n.d.	0.08	0.61	0.56	0.45	n.d.	n.d.	n.d.
Solanum-1	311.0	311.1	4	Carb/Mudst	0.96	480	36	441	0.02	0.59	0.48	0.46	0.24	n.d.	n.d.
Solanum-1	313.4	313.5	4	Carbonate	0.21	74	133	432	0.11	0.58	0.49	0.35	0.34	n.d.	n.d.
Solanum-1	315.6	315.6	4	Mudstone	3.58	763	9	438	0.02	0.59	0.53	0.58	0.21	n.d.	n.d.
Solanum-1	316.2	316.3	4	Carb/Mudst	0.58	244	99	437	0.02	0.60	0.51	0.46	n.d.	n.d.	n.d.
Solanum-1	318.9	319.0	4	Carb/Mudst	1.32	377	22	437	0.01	0.58	0.43	0.47	0.28	0.53	n.d.
Santalum-1A	449.7	449.8	4	Carbonate	0.39	131	144	431	0	n.d.	n.d.	n.d.	n.d.	n.d.	n.d.
Santalum-1A	459.3	459.4	4	Carbonate	0.42	8	89	420	0	n.d.	n.d.	n.d.	n.d.	n.d.	n.d.
Santalum-1A	466.6	466.7	4	Carbonate	0.26	38	183	425	0	0.55	0.28	0.35	0.53	0.60	n.d.
Santalum-1A	470.8	470.9	4	Carbonate	0.16	20	275	421	0	0.53	0.45	0.41	n.d.	n.d.	n.d.
Santalum-1A	474.6	474.7	4	Carbonate	0.11	148	198	n.d.	0.2	0.53	0.42	0.44	n.d.	n.d.	n.d.
Santalum-1A	478.2	478.4	4	Carbonate	0.46	147	98	434	0.01	0.58	0.26	0.42	0.45	n.d.	n.d.
Santalum-1A	485.3	485.4	4	Carbonate	0.24	28	197	423	0	0.50	0.28	0.38	n.d.	n.d.	n.d.
Santalum-1A	489.5	489.6	4	Carbonate	0.33	267	117	434	0.01	0.56	0.41	0.45	n.d.	0.55	n.d.
Goldwyer-1	873.9	876.6	4	Mudstone	0.34	59	121	432	0.05	0.58	0.50	0.31	0.41	0.79	0.46
Goldwyer-1	972.7	975.7	1+2	Mudstone	1.35	214	37	434	0.18	0.54	0.51	0.59	0.40	1.05	0.79
Goldwyer-1	975.7	980.0	1+2	Mudstone	0.35	114	131	435	0.11	0.59	0.44	0.60	n.d.	n.d.	n.d.

Goldwyer-1	980.0	983.6	1+2	Mudstone	1.37	232	29	439	0.15	0.57	0.52	0.60	0.42	1.05	0.80
Theia-1	1217.7	1217.7	4	Silty Mudst.	n.d.	n.d.	n.d.	n.d.	n.d.	n.d.	n.d.	n.d.	n.d.	n.d.	n.d.
Theia-1	1271.5	1271.5	4	Silty Mudst.	0.06	210	271	n.d.	0.04	n.d.	n.d.	n.d.	n.d.	n.d.	n.d.
Theia-1**	1276.1	1276.2	4	Silty Mudst.	n.d.	n.d.	n.d.	n.d.	n.d.	n.d.	n.d.	n.d.	n.d.	n.d.	n.d.
Theia-1**	1518.3	1518.3	1+2	Silty Mudst.	n.d.	n.d.	n.d.	n.d.	n.d.	n.d.	n.d.	n.d.	0.48	n.d.	n.d.
Theia-1**	1523.6	1523.6	1+2	Silty Mudst.	1.92	153	30	438	0.33	n.d.	n.d.	n.d.	0.49	n.d.	1.05
Theia-1**	1538.3	1538.3	1+2	Silty Mudst.	2.18	149	24	436	0.34	n.d.	n.d.	n.d.	0.52	1.29	1.13
Theia-1**	1547.1	1547.1	1+2	Silty Mudst.	3.08	154	18	435	0.35	n.d.	n.d.	n.d.	0.53	1.30	1.05
Theia-1	1552.7	1552.8	1+2	Silty Mudst.	3.15	214	11	441	0.27	n.d.	n.d.	n.d.	0.52	n.d.	n.d.
Theia-1**	1553.6	1553.6	1+2	Silty Mudst.	3.67	166	11	433	0.38	n.d.	n.d.	n.d.	0.56	1.28	1.17

*analyses performed on cuttings
**data courtesy of Finder Exploration Pty Ltd
Tmax is not reported if the S2 is <0.2 mg/g
n.d. = not determined, Mudst = mudstone
PI = production index; RockEval S1/(S1+S2)
C_{31}H S/(S+R) = C_{31} homohopane 22S/(22S+22R)
C_{29} ααα S/(S+R) = C_{29} 5α,14α,17α sterane 20S/(20S+20R)
Dia St/(dia+reg St) = ΣC_{27}-C_{29} diasteranes / ΣC_{27}-C_{29} diasteranes + ΣC_{27}-C_{29} regular steranes
MPI (methylphenanthrene index) = (3-MP+2-MP)/(3-MP+2-MP+9-MP+1-MP)
Mean faunal reflect. = average of chitinozoan and graptolite maceral reflectance
Mean bitumen reflect. =average of bitumen maceral reflectance

Table 2

		UNIT 4				UNITS 1+2		
		Goldwyer-1 873.86-876.61m	**Theia-1** 1217.67-1217.7m	**Santalum-1A** 449.7-489.6m*	**Solanum-1** 302.84-319m*	**Goldwyer-1** 972.65-975.66m	**Theia-1** 1498.8-1498.85m	**Theia-1** 1552.7-1552.75m
ACRITARCHA (spinose acritarchs)	*Rhopaliophora* spp.	X	X					
	Michrystridium sp.	X	X					
	Multiplicisphaeridium? sp.		X					
	Striatotheca indistincta (Quintavalle and Playford (2006))		X					
	Dasydorus cirritus (Playford and Martin, 1984)		X					
	Pirea sp. cf. *P. ornata* (Burmann (1970), Eisenack et al. (1976))		X					
	Sacculidium aduncum (Playford and Martin (1984) emend Ribecai et al. (2002))		X					
PRASINOPHYCEAE green algae	*Leiosphaeridia* sp.				X	X	X	
?CYANOPHYCEAE cyanobacteria	*Gloeocapsomorpha prisca* Zalessky emend Foster et al. (1989)		X	**X****	**X$_{(1)}$**			
OTHER ORGANIC-WALLED MICROFOSSILS (animal)								
chitinozoans		X	X	X	X	X	X	X
scolecodonts		X	X					
graptolite fragments		X					X	X
CRYPTOSPORES Plant	enclosed dyads		X					
	enclosed tetrads		X					
	naked ?trilete		X					

*Santalum-1A samples: 449.7–449.8 m, 459.3–459.4 m, 489.5–489.6 m, Solanum-1 samples: 302.84–303 m, 313.4–313.5 m, 311–311.12 m, 318.9–319 m

**X: dominant >95% of assemblage, X$_{(1)}$: dominant in sample from 318.9–319 m

Table 3

Well	Upper Depth (m)	Unit	Pr/ Ph	hopanes (C_{27}-C_{35})/ steranes (C_{27}-C_{29})	GA index (Ga/C_{31}H 22R)	2MHI (%)	3MHI (%)	2MeH/ 3MeH (C_{31}-C_{35})	C_{35} HHI	DNH/ 30H	TNH/ (Ts+ Tm)	DBT /P	C_{27} St (%)	C_{28} St (%)	C_{29} St (%)	C_{30} St (%)	C_{30} MeSt (%)
Solanum-1	280.04	4	0.6	12.5	0.01	7.8	7.7	1.13	0.02	0.06	0.01	n.d.	0.43	0.19	0.39	1.4	7.8
Solanum-1	284.50	4	0.8	12.3	0.01	7.4	12.2	0.67	0.03	0.06	0.01	n.d.	0.39	0.19	0.41	1.0	9.5
Solanum-1	291.60	4	0.5	3.5	0.07	10.3	7.0	1.73	0.05	0.13	0.03	0.13	0.40	0.23	0.37	2.6	9.8
Solanum-1	296.40	4	0.6	2.6	0.09	11.7	7.2	1.98	0.07	0.15	0.04	0.11	0.38	0.25	0.37	2.7	10.6
Solanum-1	302.84	4	0.3	3.1	0.06	8.8	9.6	1.01	0.05	0.14	0.03	0.07	0.43	0.23	0.34	2.3	9.5
Solanum-1	304.73	4	0.7	4.9	0.08	6.5	5.2	1.27	n.d.	0.10	n.d.	n.d.	0.40	0.27	0.34	0.0	0.0
Solanum-1	308.79	4	0.5	5.6	0.03	5.9	9.5	0.60	0.02	0.08	0.01	0.06	0.49	0.17	0.34	0.0	7.3
Solanum-1	310.30	4	0.6	6.6	0.04	7.5	5.8	1.32	0.02	0.08	n.d.	n.d.	0.49	0.17	0.34	0.0	0.0
Solanum-1	311.00	4	0.9	8.5	0.01	7.2	14.9	0.52	0.04	0.05	0.00	0.01	0.39	0.18	0.43	0.9	9.2
Solanum-1	313.40	4	0.4	3.0	0.08	11.5	6.6	2.04	0.08	0.13	0.04	0.08	0.36	0.25	0.39	3.1	11.0
Solanum-1	315.58	4	1.2	10.9	0.02	3.5	12.7	0.25	0.02	0.01	0.00	0.03	0.49	0.14	0.36	0.0	4.4
Solanum-1	316.20	4	1.0	6.1	0.04	3.4	9.1	0.35	0.03	0.06	0.02	0.06	0.49	0.18	0.32	1.6	6.3
Solanum-1	318.90	4	1.1	6.7	0.07	5.5	10.6	0.46	0.04	0.06	0.01	0.01	0.41	0.21	0.38	0.7	9.1
Santalum-1A	449.73	4	1.8	n.d.	n.d.	n.d.	n.d.	n.d.	n.d.	n.d.	n.d.	0.02	n.d	n.d	n.d	n.d	n.d
Santalum-1A	459.30	4	0.8	6.6	n.d.	n.d.	n.d.	n.d.	n.d.	n.d.	n.d.	n.d.	n.d	n.d	n.d	n.d	n.d
Santalum-1A	466.59	4	1.4	6.7	0.03	7.8	14.0	0.58	0.03	0.12	n.d.	n.d.	0.33	0.21	0.46	0.0	0.0
Santalum-1A	470.82	4	1.4	6.0	0.03	5.9	5.6	1.32	0.02	0.06	0.01	0.22	0.44	0.18	0.38	0.0	0.0
Santalum-1A	474.60	4	1.6	5.7	0.03	4.8	9.2	0.66	0.03	0.06	0.01	0.07	0.47	0.21	0.31	0.0	0.0
Santalum-1A	478.19	4	1.7	8.4	0.02	5.5	16.5	0.37	0.02	0.08	0.00	n.d.	0.38	0.19	0.44	0.0	5.3
Santalum-1A	485.30	4	1.0	9.2	0.02	8.1	15.7	0.54	0.03	0.10	n.d.	n.d.	0.30	0.18	0.52	0.0	0.0
Santalum-1A	489.50	4	1.7	5.2	0.05	6.7	8.9	0.76	n.d.	0.05	0.01	0.06	0.48	0.20	0.32	0.0	0.0
Goldwyer-1	873.86	4	1.8	1.8	0.09	5.1	2.5	1.95	0.03	0.18	0.03	0.03	0.50	0.27	0.22	0.9	4.3
Goldwyer-1	972.65	1+2	0.6	2.0	0.33	7.0	2.7	8.04	0.07	0.07	0	0.03	0.35	0.18	0.47	0.0	8.6

Goldwyer-1	975.66	1+2	0.9	1.5	0.36	4.5	2.2	3.86	0.03	0.04	0	n.d.	0.31	0.14	0.54	0.0	0.0
Goldwyer-1	979.97	1+2	1.0	1.5	0.73	6.7	4.6	7.08	0.07	0.13	0	0.03	0.36	0.18	0.46	0.0	9.5
Theia-1	1217.7	4	1.6	n.d.	n.d.	n.d.	n.d.	n.d.	n.d.	n.d.	n.d.	0.10	n.d.	n.d.	n.d.	n.d.	n.d.
Theia-1	1271.48	4	1.1	1.6	n.d.	n.d.	n.d.	n.d.	n.d.	n.d.	n.d.	0.14	n.d.	n.d.	n.d.	n.d.	n.d.
Theia-1**	1276.1	4	1.5	3.0	n.d.	n.d.	n.d.	n.d.	n.d.	n.d.	n.d.	0.14	n.d.	n.d.	n.d.	n.d.	n.d.
Theia-1**	1518.26	1+2	1.5	n.d.	n.d.	n.d.	n.d.	n.d.	n.d.	n.d.	n.d.	0.08	n.d.	n.d.	n.d.	n.d.	n.d.
Theia-1**	1523.56	1+2	1.1	n.d.	n.d.	n.d.	n.d.	n.d.	n.d.	n.d.	n.d.	0.06	n.d.	n.d.	n.d.	n.d.	n.d.
Theia-1**	1538.28	1+2	1.4	n.d.	n.d.	n.d.	n.d.	n.d.	n.d.	n.d.	n.d.	0.04	n.d.	n.d.	n.d.	n.d.	n.d.
Theia-1**	1547.07	1+2	1.4	n.d.	n.d.	n.d.	n.d.	n.d.	n.d.	n.d.	n.d.	0.04	n.d.	n.d.	n.d.	n.d.	n.d.
Theia-1	1552.70	1+2	1.4	n.d.	n.d.	n.d.	n.d.	n.d.	n.d.	n.d.	n.d.	0.06	n.d.	n.d.	n.d.	n.d.	n.d.
Theia-1**	1553.59	1+2	1.6	n.d.	n.d.	n.d.	n.d.	n.d.	n.d.	n.d.	n.d.	0.04	n.d.	n.d.	n.d.	n.d.	n.d.

**data courtesy of Finder Exploration Pty Ltd
n.d. = not determined
Pr/Ph = Pristane/Phytane
Gammacerane index = Gammacerane/C_{31}hopane 22R
2MHI = 2α-methyl C_{30} hopane/(2α-methyl C_{30} hopane + C_{30} hopane) × 100
3MHI = 3β-methyl C_{30} hopane/(3β-methyl C_{30} hopane + C_{30} hopane) × 100
2MH/3MH = 2α-methylhopanes/3β-methylhopanes (C_{31} - C_{35})
C_{35} homohopane index = C_{35} homohopanes (22S+R)/Σ(C_{31}-C_{35} homohopanes (22S+R))
DNH/30H = 28,30-*dinor*hopane/C_{30} 17α,21β(αβ) hopane
TNH/(Ts+Tm) = 25,28,30-*trisnor*hopane/(18α22,29,30-*trisnor*hopane+17α22,29,30-*trisnor*hopane)
DBT/P = dibenzothiophene/phenanthrene
C_{27} St (%) = C_{30} steranes/ΣC_{27}–C_{29} steranes × 100
C_{28} St (%) = C_{30} steranes/ΣC_{27}–C_{29} steranes × 100
C_{29} St (%) = C_{30} steranes/ΣC_{27}–C_{29} steranes × 100
C_{30} St (%) = C_{30} steranes/ΣC_{27}–C_{30} steranes × 100
C_{30} MeSt (%) = abundance of selected methylated 24-ethylcholestanes (2α-, 3β-, 4α- and 4β-)/(ΣC_{27}–C_{29} steranes + C_{30} methylsteranes) × 100

Table 4

Well	Upper Depth (m)	Short-chain *n*-alkanes								Long-chain *n*-alkanes									
		C_{14}	C_{15}	C_{16}	C_{18}	C_{19}	C_{20}	C_{21}	C_{22}	C_{23}	C_{24}	C_{25}	C_{26}	C_{27}	C_{28}	C_{29}	C_{30}	C_{31}	C_{32}
Santalum-1A	459.3				-27.1	-27.8	-27.7	-27.4	-28.2	-29.3		-31.1							
Santalum-1A	466.6		-28.8	-27.7	-28.3	-27.9	-27.6	-28.1	-28.4	-28.4	-29.4	-30.1	-29.9	-30.3	-30.5	-31.1		-32.1	-32.3
Santalum-1A	470.8			-27.8		-27.7	-27.7	-28.1	-28.6	-29.2	-30.0	-30.7			-30.7	-31.0			
Santalum-1A	474.6	-29.2		-27.2		-27.8	-27.3			-30.5	-31.0	-31.8	-31.8	-31.5	-31.7		-31.6	-32.1	-32.5
Santalum-1A	478.2	-28.2	-27.7	-27.1	-27.9	-29.4		-29.5	-30.7	-31.9	-31.5	-32.0	-31.2	-31.5		-32.0	-32.0	-31.7	
Santalum-1A	485.3		-28.8	-27.8	-27.4	-28.1	-28.4		-29.7		-30.9	-30.5		-30.6		-30.9		-31.4	
Solanum-1	280.0				-27.8	-28.5	-29.1		-29.0	-29.5									
Solanum-1	284.5				-29.4														
Solanum-1	291.6					-28.3	-27.9		-28.1										
Solanum-1	296.4			-28.6	-27.8	-28.4	-28.4	-27.6		-27.6			-27.6	-28.6					
Solanum-1	302.8				-28.5			-28.8	-28.7	-28.2	-29.7	-29.7							
Solanum-1	308.8				-27.3	-28.8				-28.8									
Solanum-1*	311.0	-31.6	-31.6	-30.0	-31.3	-30.1	-31.5	-30.5											
Solanum-1	313.4				-27.9		-28.5					-28.9			-28.3				
Solanum-1*	315.6	-31.9	-31.6	-30.3		-31.4													
Solanum-1	316.2		-30.4	-30.3		-30.2	-29.7												
Solanum-1*	318.9	-31.3	-31.4	-31.0	-30.2	-31.3	-30.0	-30.4											
Goldwyer-1	873.9		-29.1	-28.5	-28.4	-29.0	-29.2			-30.0									
Goldwyer-1	972.7	-31.9	-32.2	-31.7	-31.7	-32.1	-33.0	-33.5	-32.7	-33.8		-32.6							
Goldwyer-1	980.0	-32.2	-32.3	-31.4			-32.4	-32.6		-32.2	-32.4	-32.7	-32.3		-32.4				
Theia 1	1557.2	-32.0		-32.5		-31.1	-31.9	-31.9		-33.0	-33.7	-33.4							

*$\delta^{13}C$ of *n*-C_{17} could be measured due to extremely low abundance of pristane, data is shown in figure 12. In all other samples *n*-C_{17} co-eluted with pristane

Table 5

Molecular signature	Identified in	Biological & environmental interpretation	Further info & references
OEP *n*-C_{15} to *n*-C_{19}	Solanum-1 (311m, 316–319m), Theia-1 (1271.5m)	*G. prisca*, marine organism of uncertain affinity	Hoffmann et al. (1987), Blokker et al. (2001)
Mid to long chain (C_{23}–C_{32}) *n*-alkanes	Santalum-1A	plant inputs (bryophytes or aquatic macrophytes)	Ficken et al. (2000)
C_{30}-hopanes, homohopanes	all samples, at varying abundances	diagnostic for the domain Bacteria	Brocks and Summons (2014)
2α-methylhopanes	all samples, at varying abundances	generally diagnostic for cyanobacteria in Phanerozoic marine deposits	Summons et al. (1999), Ricci et al. (2014, 2015)
3β-methylhopanes	all samples, at varying abundances	diagnostic for certain methylotrophs, methanotrophs and acetic acid bacteria	Summons and Jahnke (1990), Welander and Summons (2012)
Gammacerane	all samples, higher abundance in Goldwyer-1 (973–984m)	water column stratification	Sinninghe Damsté et al. (1995)
C_{27}–C_{29} steranes	all samples, at varying abundances	primarily diagnostic for eukaryotes in marine deposits	Brocks and Summons, 2014
24-*n*-propylcholestane (C_{30})	Solanum-1, Goldwyer-1 (874–876m)	Pelagophyte algae, a biomarker for marine conditions	Moldowan et al. (1990)
Dinosterane (4α,23,24-trimethylcholestane)	Solanum-1, Goldwyer-1	A biomarker for acritarchs (dinoflagellate biomarker in post Triassic sediments)	Fensome et al. (1996), Moldowan and Talyzina (1998), Talyzina et al. (2000), Arouri et al. (2000)
4α-methyl-24-ethylcholestanes	Solanum-1, Goldwyer-1	A biomarker for acritarchs (dinoflagellate biomarker in post Triassic sediments)	
OEP long-chain alkylnaphthalenes (C_{21}, C_{23})	Solanum-1 (280–319m), Santalum-1A (449.7m)	*G. prisca*, marine organism of uncertain affinity	Fowler et al. (2004)
Benzonaphthofurans	Theia-1 (1217.6m)	? plant-derived	Li and Ellis (2015)
Isorenieratane, Palaerenieratane	Solanum-1 (316.2–316.3m), Theia-1 (1552.7–1552.75m)	Green sulphur bacteria, photic zone euxinia	Brocks and Summons (2014)
Isotopic signature			
^{13}C depleted *n*-C_{17} and *n*-C_{19} (–31.4‰) compared to *n*-C_{16} and *n*-C_{18} (–30.0‰)	Solanum-1 (311m, 316–319m)	*G. prisca* utilised a ^{13}C depleted carbon source (possibly from methanotrophs)	
^{13}C depleted *n*-$C_{23–32}$ relative to *n*-$C_{16–19}$	Santalum-1A	isotopic discrepancy greater than in other samples, mid-chain *n*-alkanes attributed to a (land) plant input	

Table 6

Well	Upper Depth (m)	Unit	$\delta^{13}C$ (*n*-$C_{16\text{-}19}$)	$\delta^{13}C$ (*n*-$C_{23\text{-}32}$)	Δ
Santalum-1A	459.3	4	–27.5	–30.2	2.8
Santalum-1A	466.6	4	–27.9	–30.2	2.3
Santalum-1A	470.8	4	–27.7	–30.3	2.6
Santalum-1A	474.6	4	–27.5	–31.5	4.0
Santalum-1A	478.2	4	–28.2	–31.7	3.6
Santalum-1A	485.3	4	–27.8	–30.9	3.1
Solanum-1	280.0	4	–28.2	–29.5	1.3
Solanum-1	291.6	4	–28.3		
Solanum-1	296.4	4	–28.3	–27.9	–0.3
Solanum-1	302.8	4	–28.5	–29.2	0.7
Solanum-1	308.8	4	–28.1	–28.8	0.7
Solanum-1	313.4	4	–27.9	–28.6	0.7
Solanum-1	311.0	4	–30.5		NA*
Solanum-1	315.6	4	–30.8		NA*
Solanum-1	316.2	4	–30.2		NA*
Solanum-1	318.9	4	–30.8		NA*
Goldwyer-1	873.9	4	–28.6	–30.0	1.3
Goldwyer-1	972.7	1+2	–31.8	–33.2	1.4
Goldwyer-1	980.0	1+2	–31.4	–32.4	0.9
Theia-1	1557.2	1+2	–31.8	–33.3	1.5

NA = not applicable, these samples display a strong *G. prisca n*-alkane signature (Fig. 4a)

Figures

Figure 1

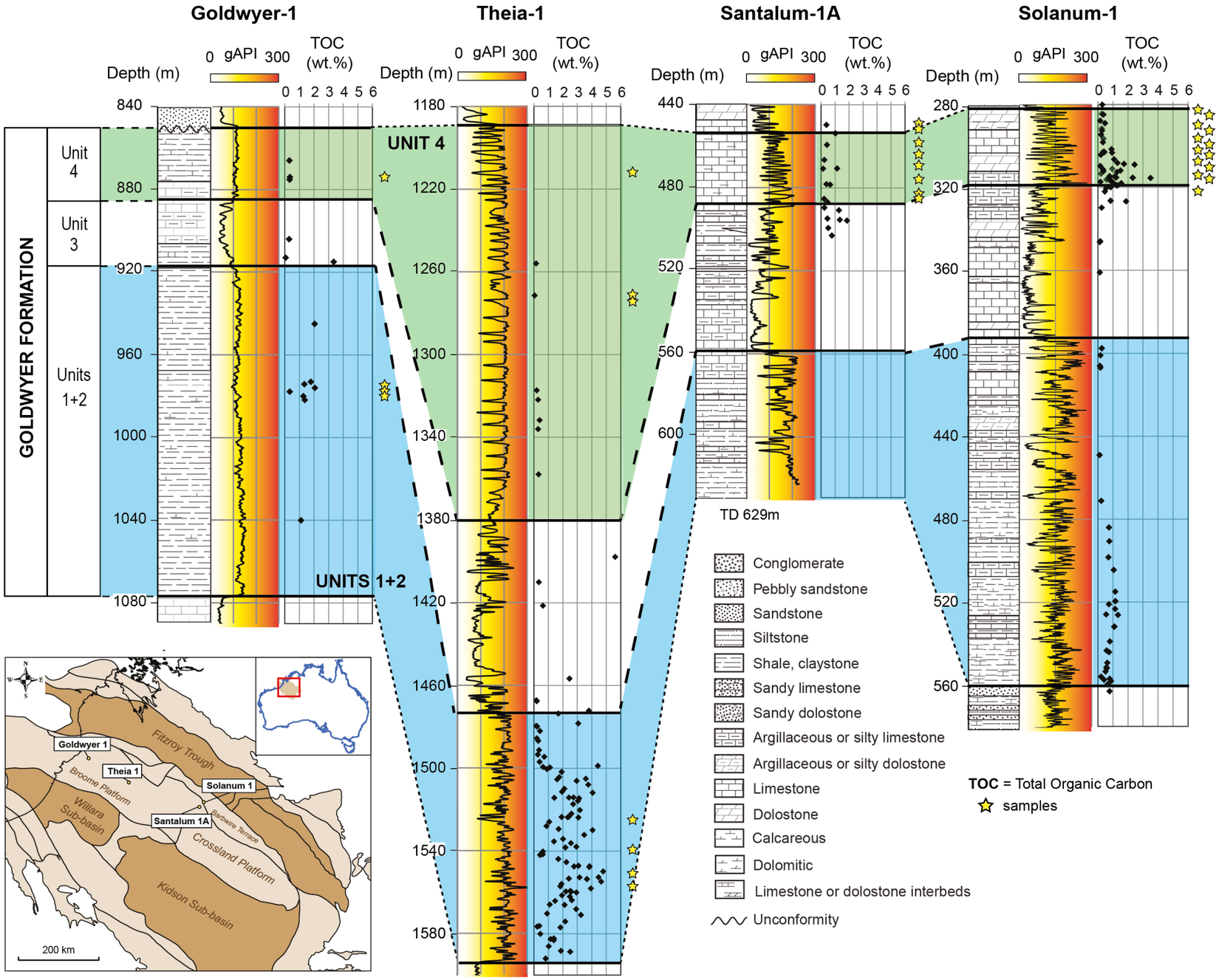

Figure 2

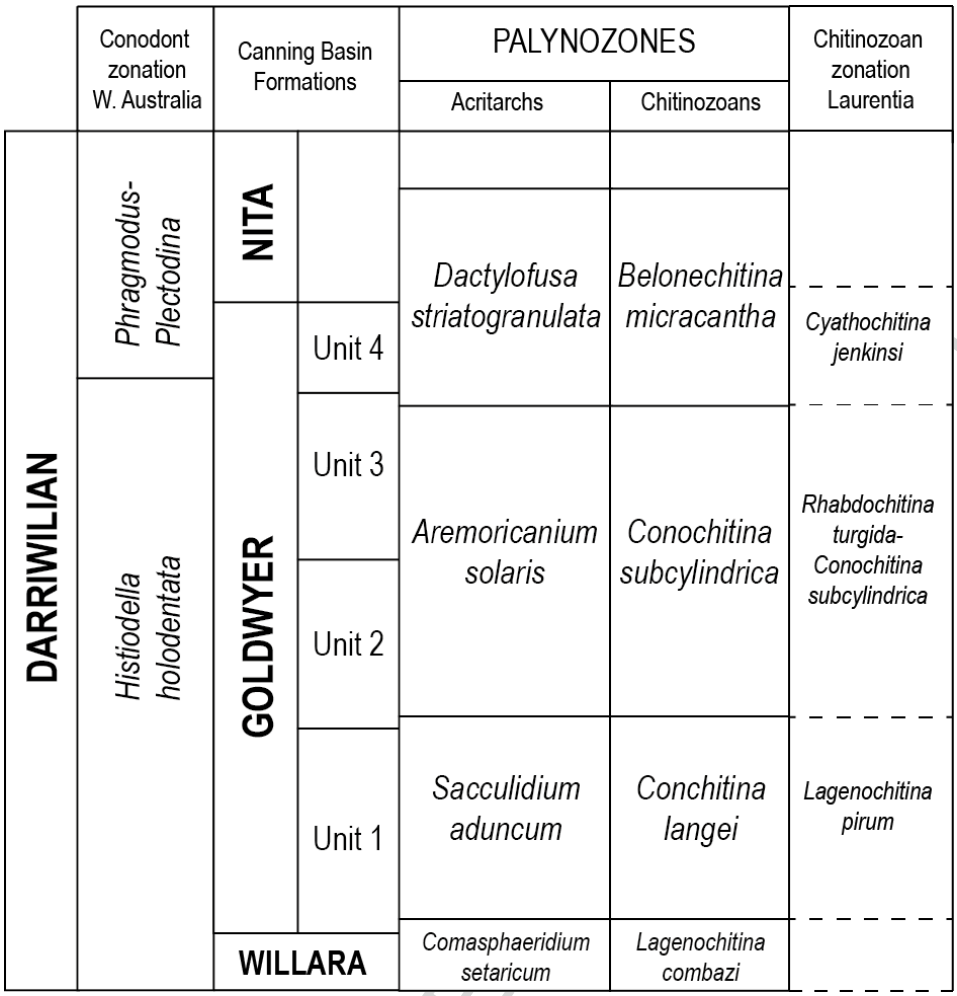

Figure 3

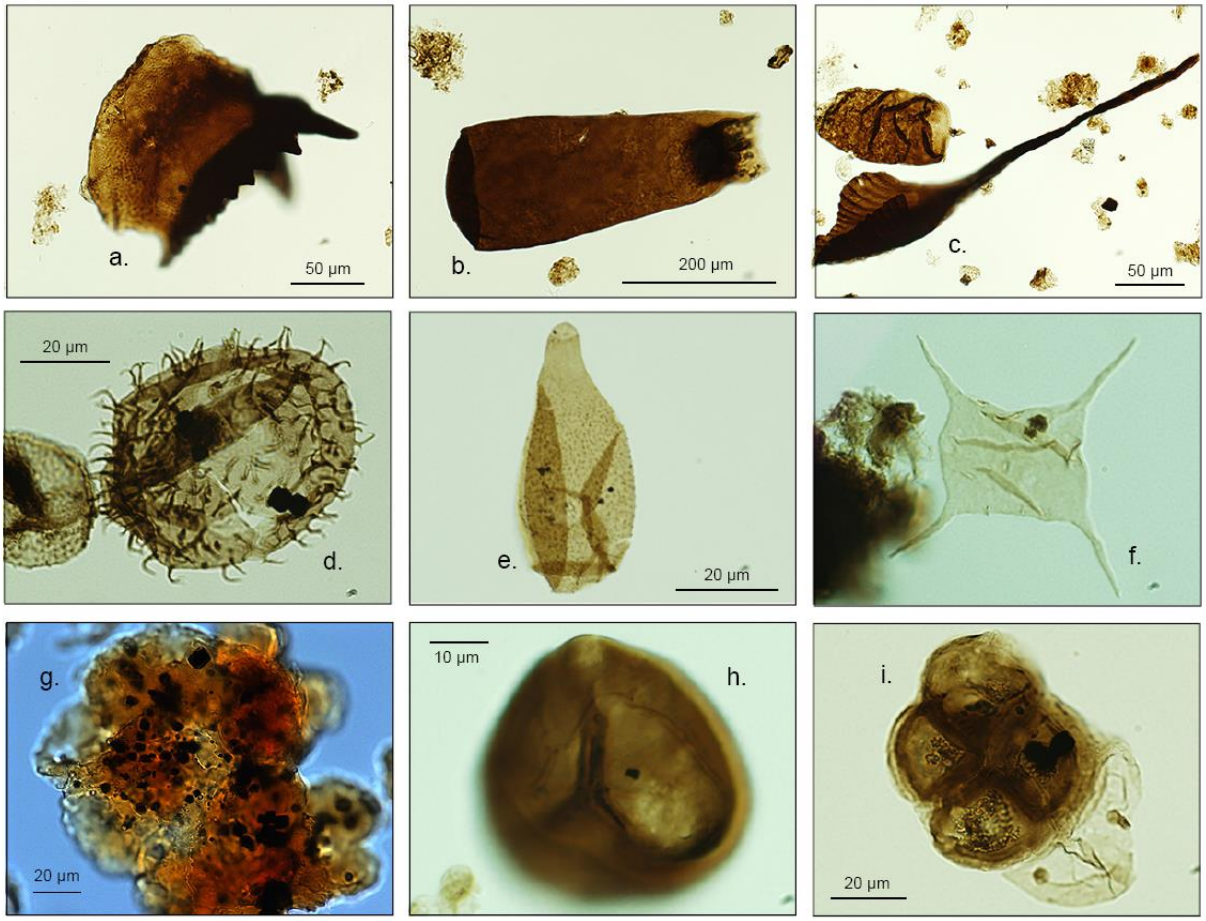

Figure 4

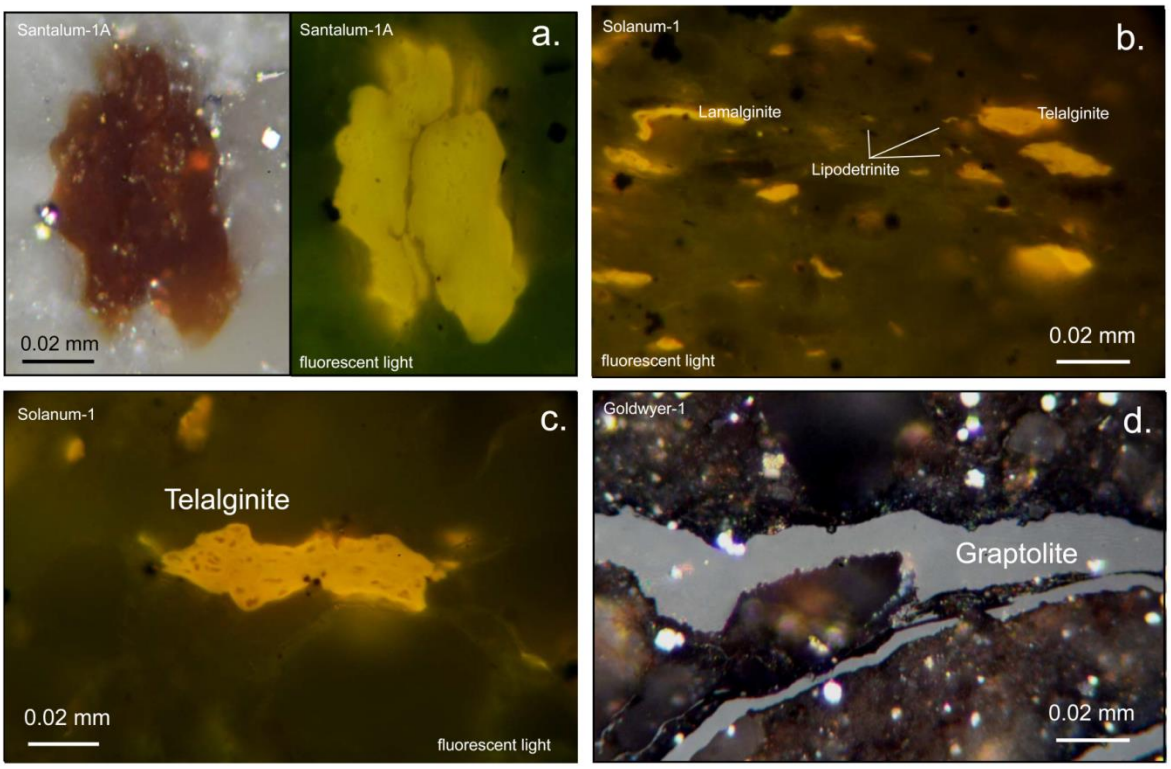

Figure 5

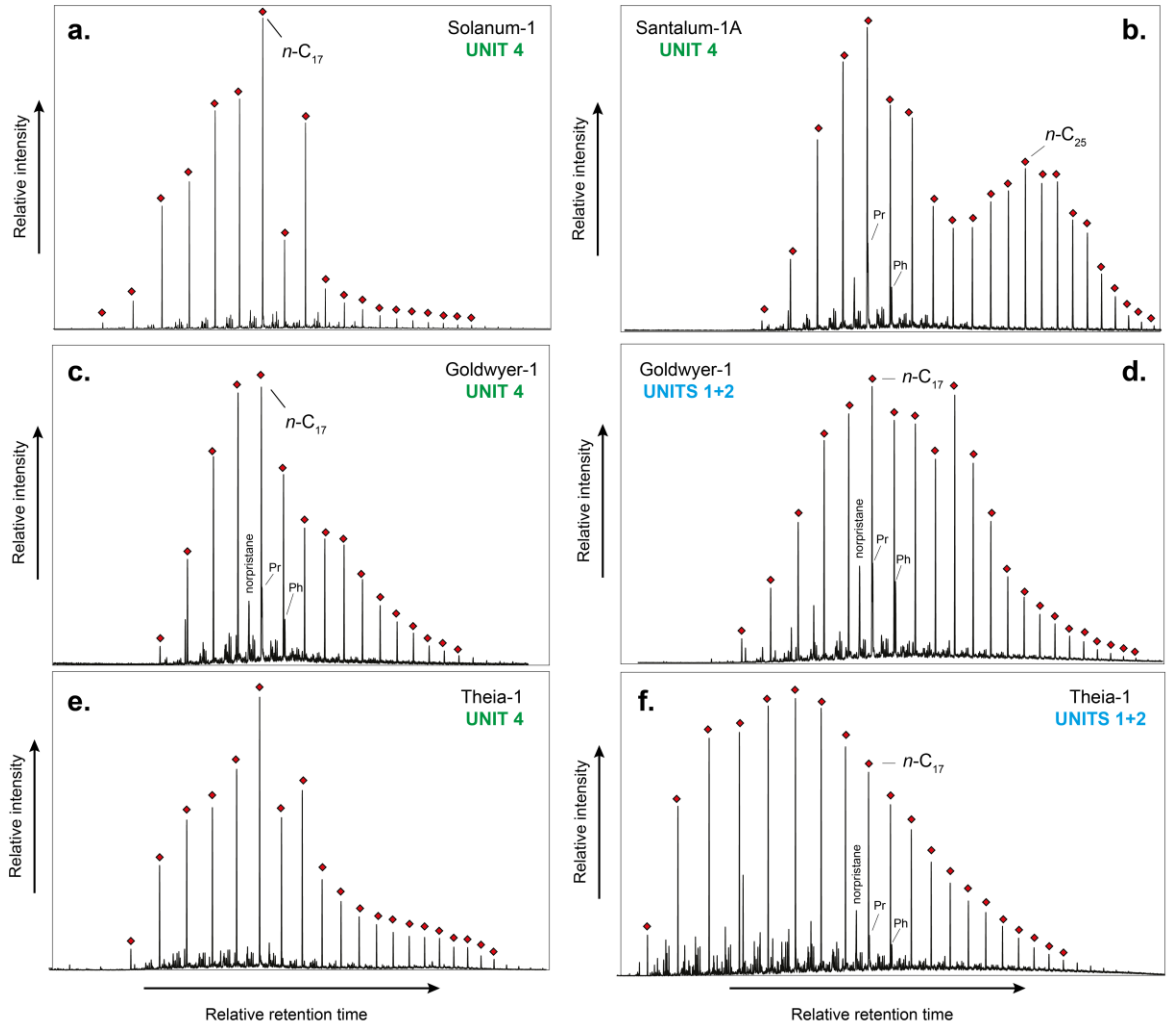

Figure 6

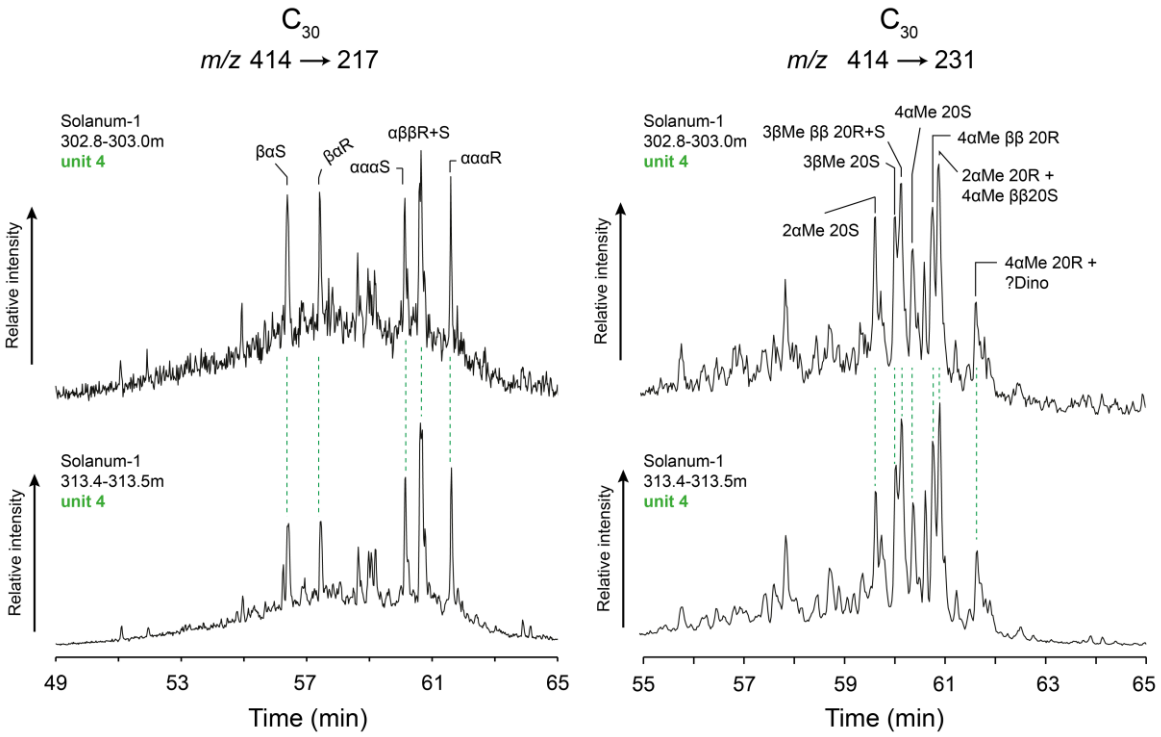

Figure 7

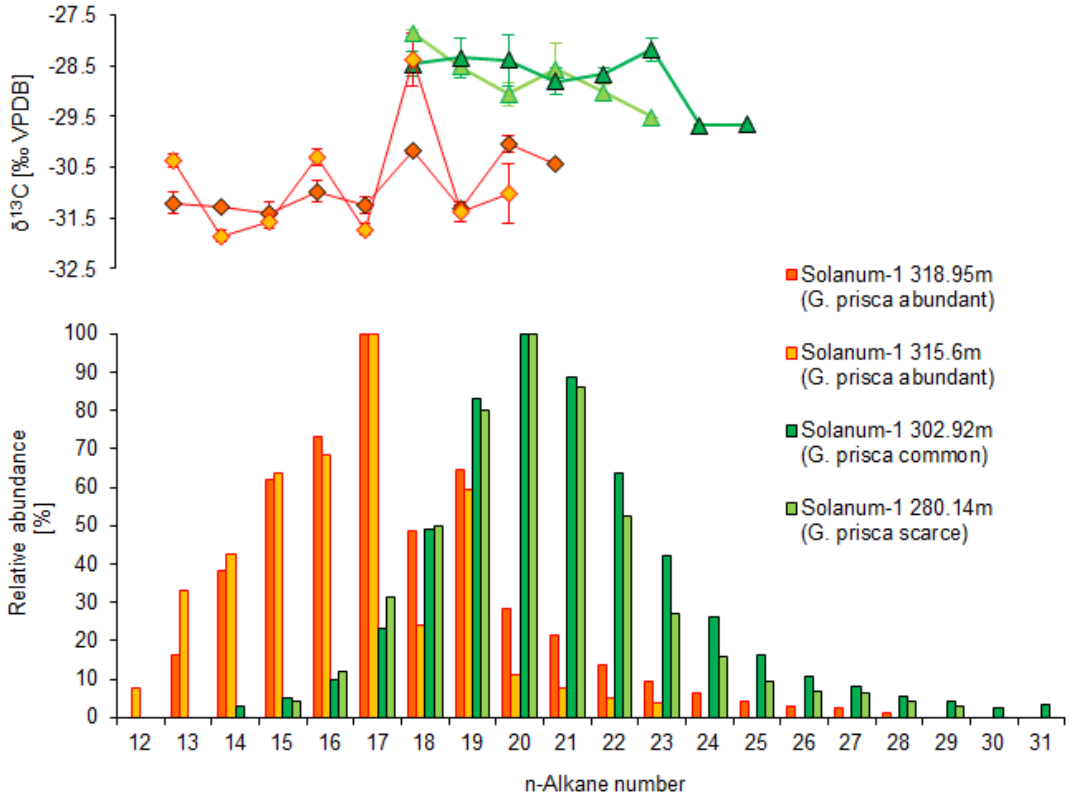

Figure 8

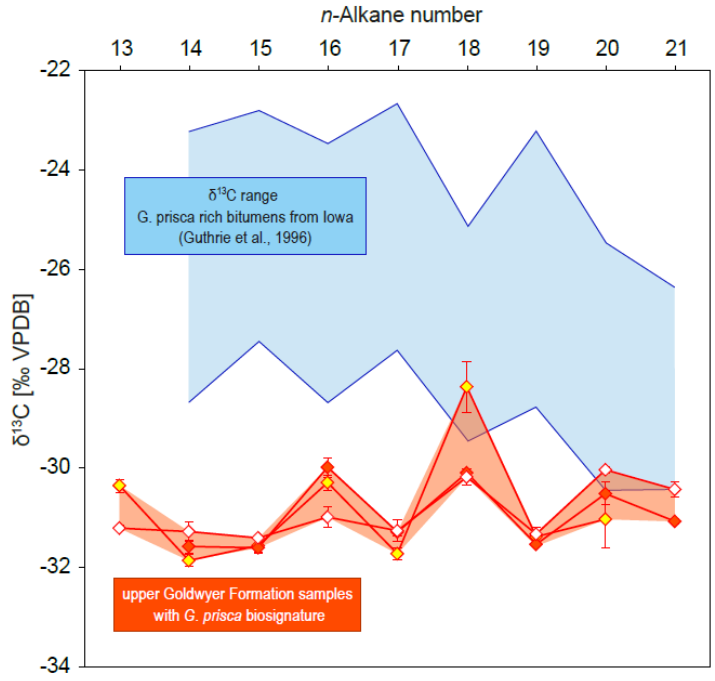

Figure 9

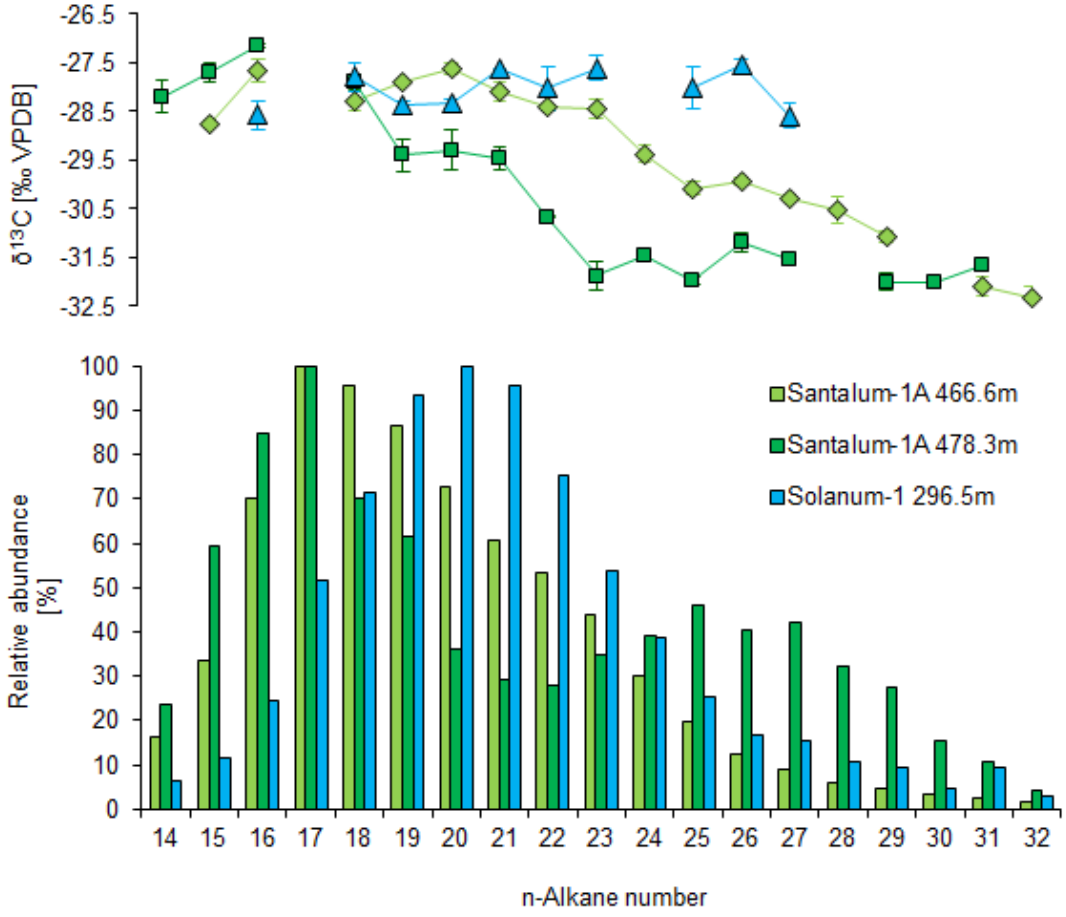

Figure 10

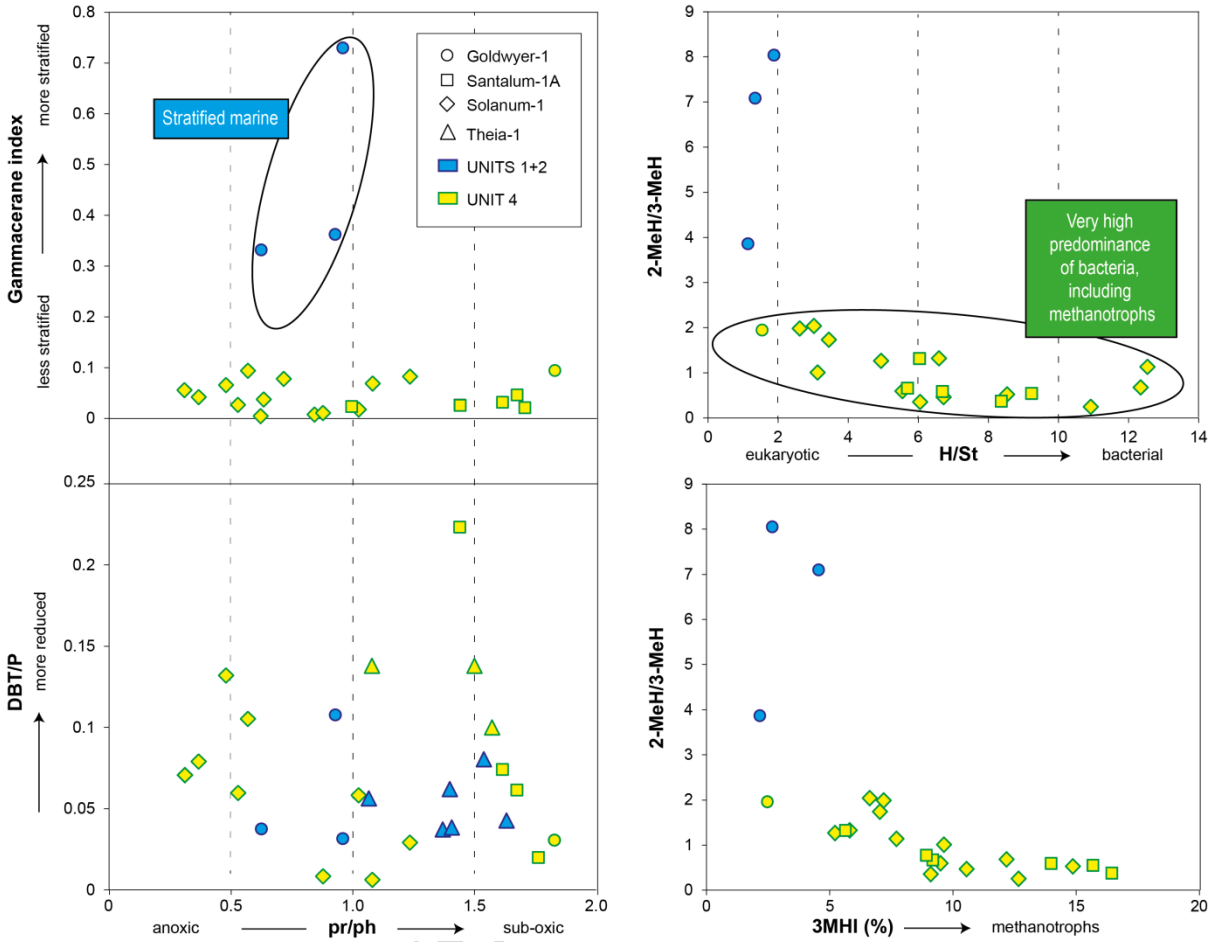

Figure 11

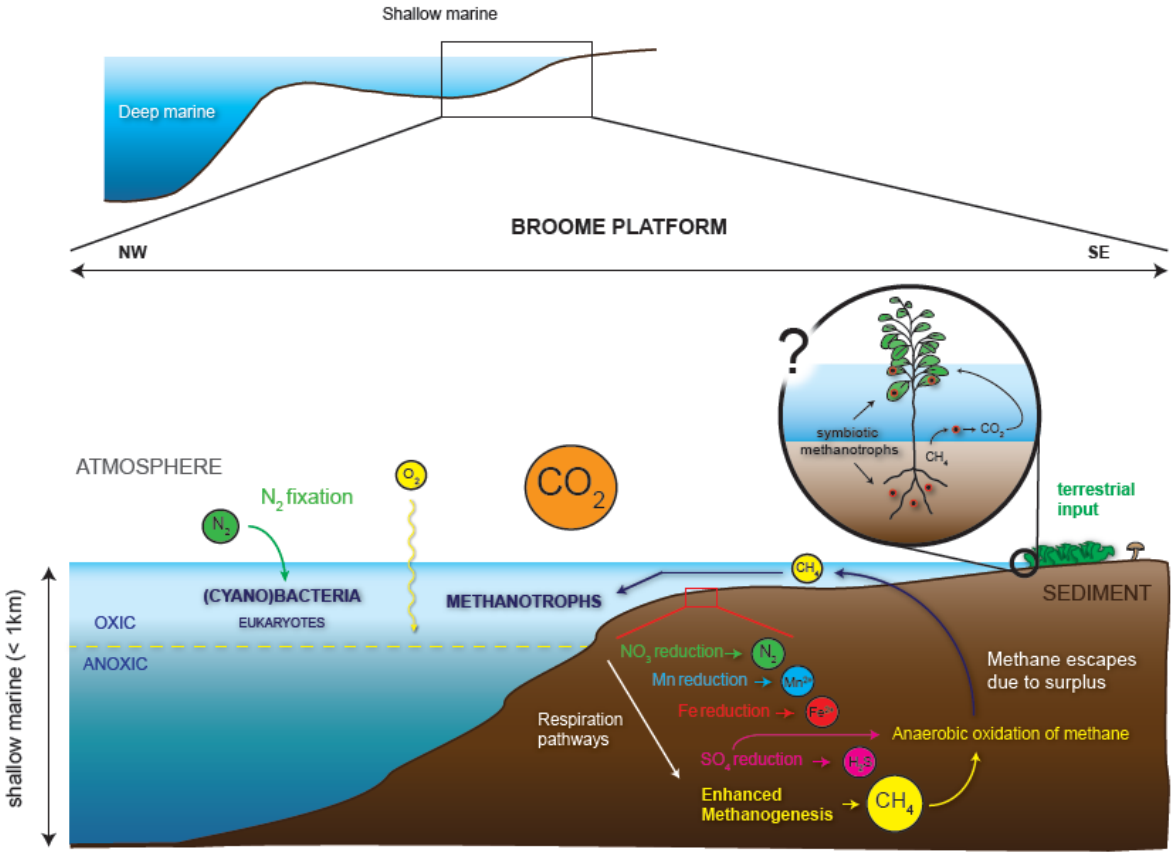

Figure 12

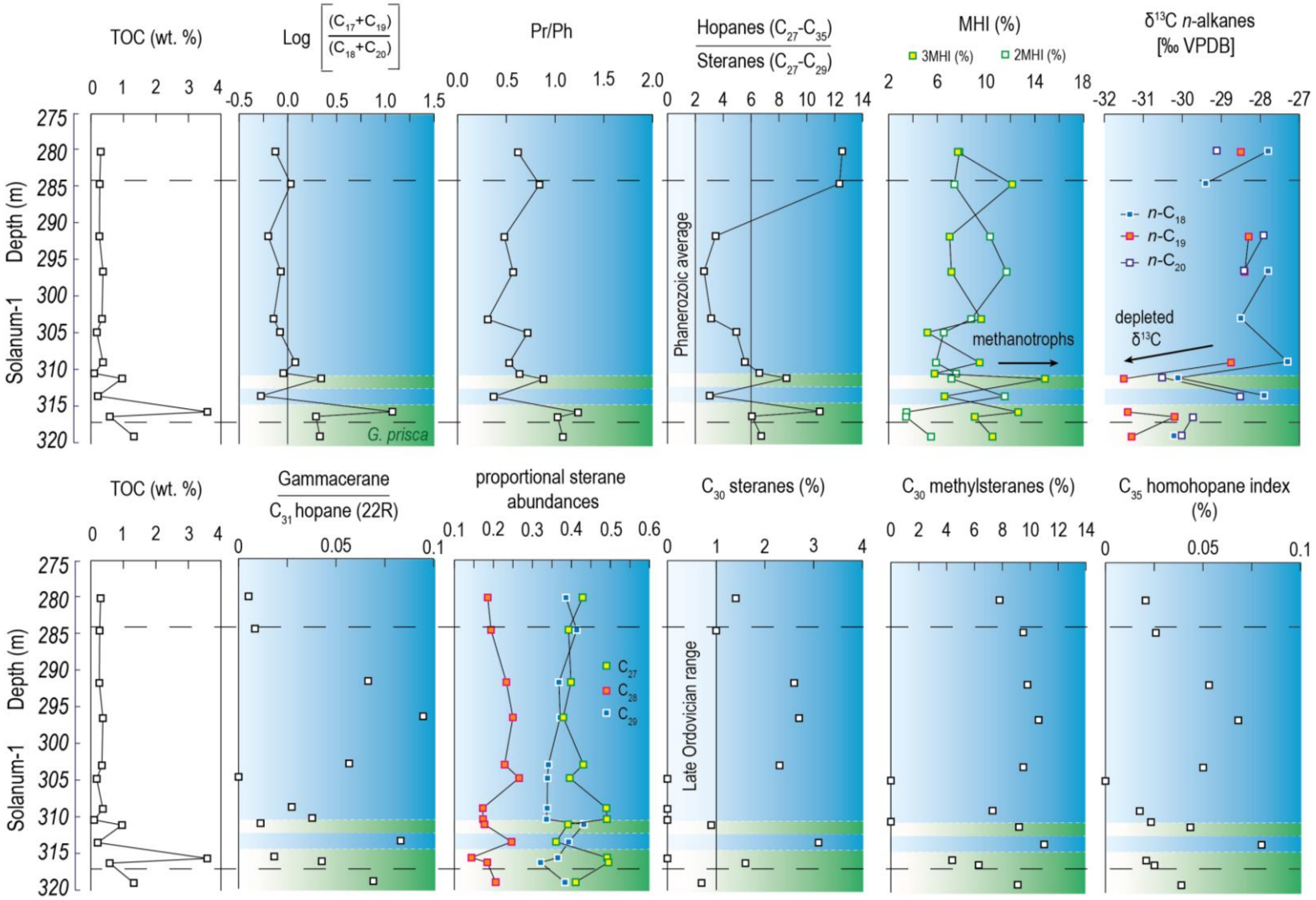

Figure 13

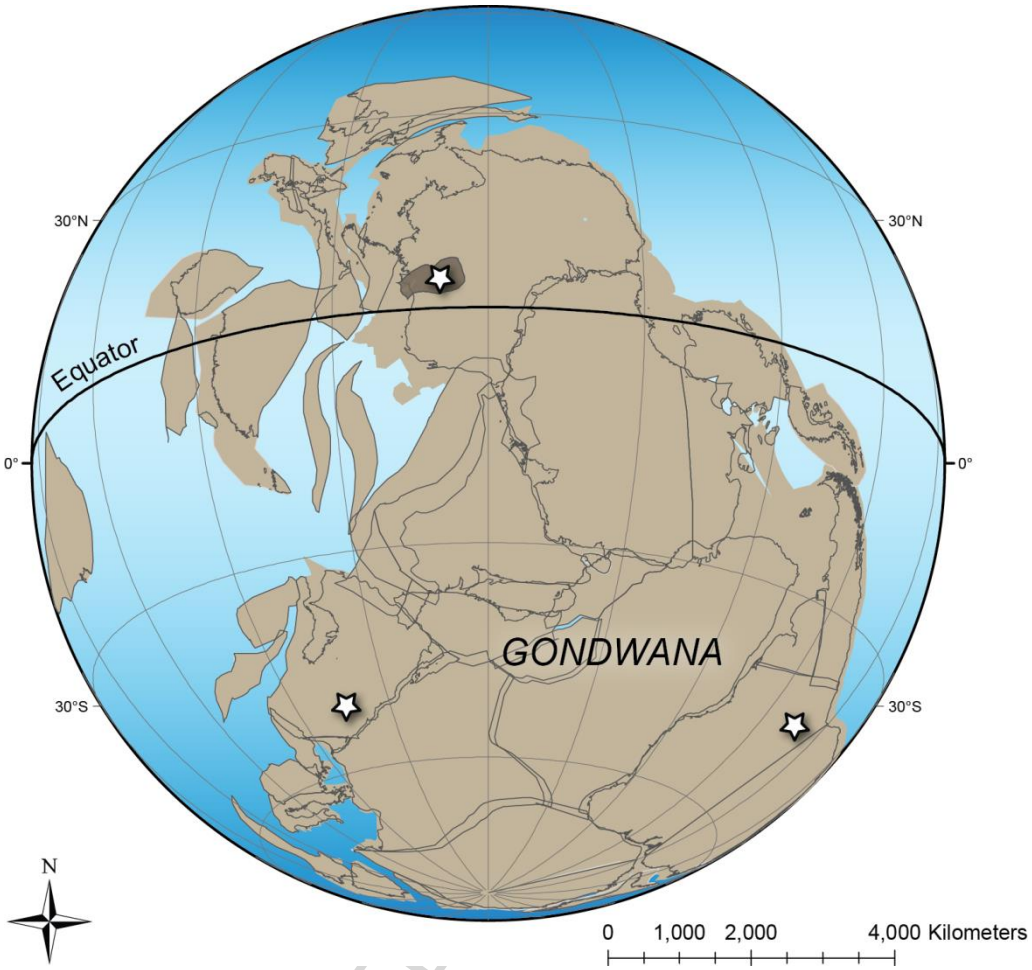

Highlights

- Oldest cryptospores in Australia reported in the Mid-Ordovician Goldwyer Formation.
- Biomarker assemblages corroborate a marine environment with land-plant input.
- Changes in microbial communities follow redox conditions.
- Enhanced methane cycling and abundant methanotrophic activity.